*Proc. Natl. Sci. Counc. ROC(A)*
Vol. 18, No. 2, 1994. pp. 119-150

*(Review Paper)*

# Airflow over Mesoscale Heat Sources Part II: Responses in a Shear Flow

YUH-LANG LIN

*Department of Marine, Earth, and Atmospheric Sciences*
*North Carolina State University*
*Raleigh, North Carolina 27695-8208, U.S.A.*

(Received November 23, 1992; Accepted June 22, 1993)

**ABSTRACT**

In part II of this series of papers, we review the responses of a stably stratified shear flow to a thermal forcing. Observations indicate that this type of shear flow is closely related to a number of mesoscale circulations. The mathematical method for solving a two-dimensional shear flow with a critical level to a prescribed thermal forcing is described. The mathematical problem is then extended to a three-dimensional flow and applied to the dynamics of mesoscale circulation associated with a mesoscale convective system. Generation and propagation of internal gravity waves by the heating are discussed. The mathematical problem is then extended to solve a stably stratified flow over a meso-$\alpha/\beta$ scale heat source. The vertical flux of horizontal momentum and wave energy associated with the thermally forced inertia-gravity waves are discussed. Both quasi-geostrophic and semi-geostrophic approaches to the problem are also reviewed. The solution is then applied to help understand the dynamics of coastal cyclogenesis.

**Key Words**: smalls flow, meso-$\alpha/\beta$ scale, meso-$\gamma$ scale, critical level, barotropic flow, quasi-geostrophic, semi-geostrophic, baroclinic wave

## I. Introduction

In part I of this series of papers, the responses of a stably stratified uniform airflow to mesoscale thermal forcing have been reviewed. Observations indicate that a number of mesoscale circulations are related to a shear flow over a heat source. Occasionally, there exists a critical level in a flow over a heat source or sink. One example is the moist convection associated with midlatitude squall lines (e.g., Thorpe *et al.*, 1982; Seitter and Kuo, 1983; Raymond, 1984). For the squall line analyzed by Ogura and Liou (1980), the rightward mode exhibits a critical level near 6 km (Fig. 1). That is, the propagation speed of the disturbance coincides with the environmental wind speed at that level. Similar phenomena have also been found in climatological studies by Bluestein and Jain (1985; see Fig. 2) and Wyss and Emanuel (1988). Thus, there exists thermal forcing below and above the critical level as the condensational heating may extend to a height of 10 km. Notice that the critical level coincides with the level of wind reversal in a steady state flow. Similar processes can also be found for moist southwesterly monsoon currents over the Western Ghats of India during the summer (Figs. 13 and 14 of Part I; Ramage, 1971; Smith and Lin, 1983). Perpendicular to the coast line, the basic flow reverses in the middle troposphere.

In some cases, the thermal forcing exists solely below the critical level. For example, this problem is relevant to the formation of a squall line in the vicinity of a dry line over the southern Great Plains (Rhea, 1966). The mesoscale circulation across the dry line favorable for the formation and maintenance of a squall line analyzed by Ogura and Chen (1977) and simulated by Sun and Ogura (1979) appears to

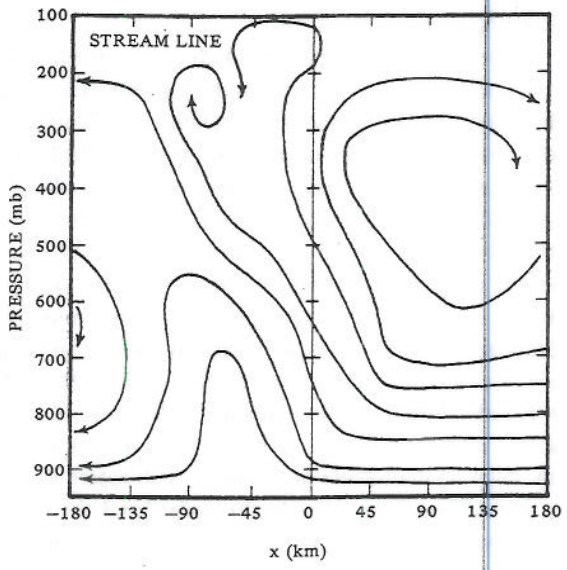


**Fig. 1.** Streamlines for a midlatitude squall line on 22 May 1976. Three important features are shown: (a) upshear tilt of the updraft, (b) downdraft fed by the front-to-rear flow, and (c) flow overturning in the middle layer. (From Ogura and Liou, 1980)

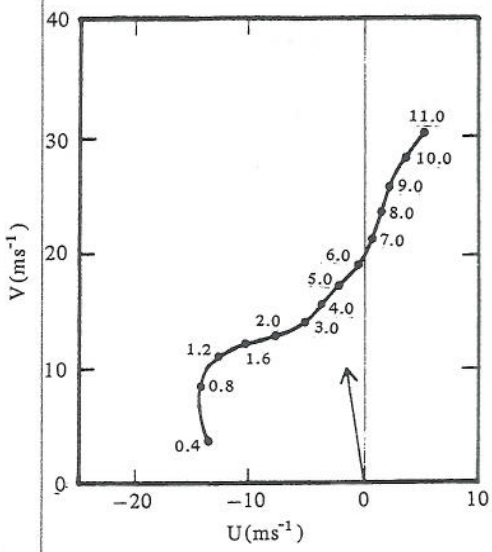


**Fig. 2.** Composite hodographs in a frame of reference moving along with squall lines averaged over an 11 year period in Oklahoma. (From Bluestein and Jain, 1985)

have a wind reversal near a low-level inversion (e.g., see Figs. 6c and 10b in Sun and Ogura). Sun and Ogura also found that upward motion is generated with sufficient intensity to release the potential instability if the synoptic-scale low-level wind is incident from the proper direction. Numerical studies of sea breeze circulation (e.g., Estoque, 1962) also indicate that the location and shape as well as the intensity of sea breeze circulation are strongly affected by the direction of the prevailing synoptic wind. Therefore, it is important to investigate the response of a continuously stratified shear flow with a critical level to prescribed heating or cooling.

The above mentioned problem may be further applied to the mesoscale flow in the vicinity of the coastal region of the Carolinas during the winter when a cold synoptic-scale anticyclone exists to the north of this region. The horizontal basic wind normal to the coastline reverses at about 2 km as the inland low-tropospheric flow underlies the westerlies in the middle and upper troposphere (Fig. 3). The low-level sensible and latent heating associated with the strong temperature contrast provides an important energy source for the mesoscale circulation, which can produce a subsynoptic scale cyclone near the surface (Lin, 1989b, 1990a). Since the Rossby number associated with the flow is less than one, the response is quite different from that of a stratified flow over a small-scale heat source with rotational effects ignored. Therefore, in order to understand the dynamics of a flow over a meso-$\alpha/\beta$ scale heat source, the effects of planetary rotation as well as baroclinicity must be included.

In Section II, the response of a continuously stratified shear flow with a critical level to a meso-$\gamma$ scale heat

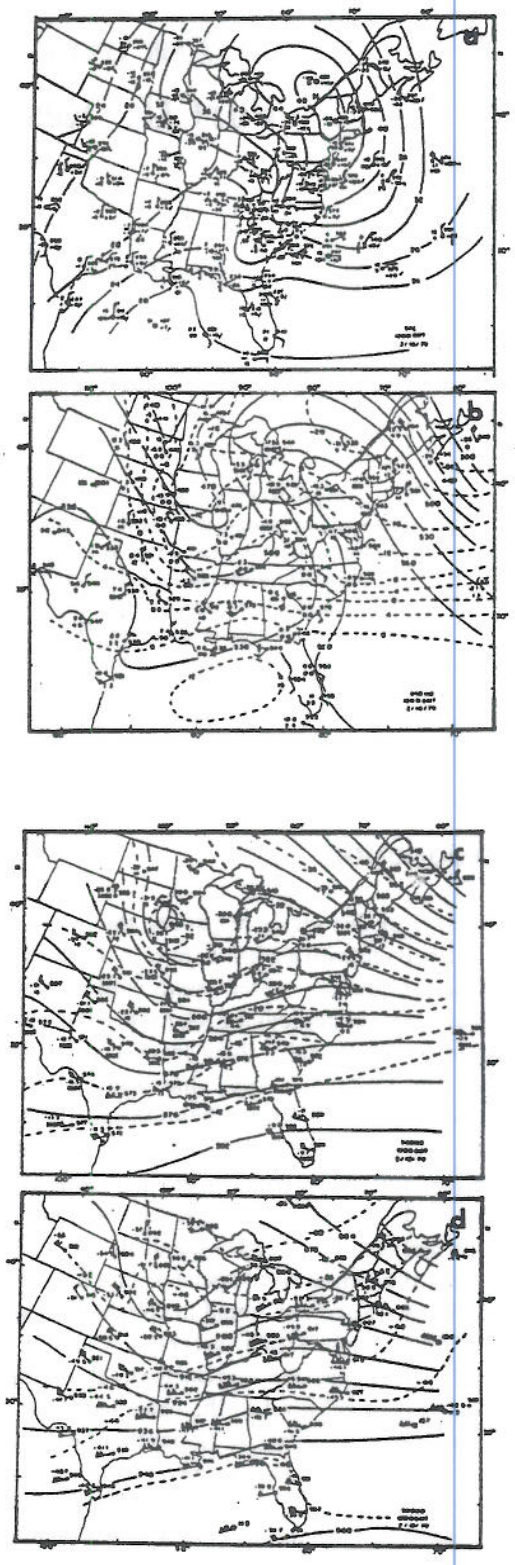


**Fig. 3.** (a) Surface, (b) 850, (c) 500 and (d) 300 mb maps for 1200 GMT 18 February Presidents' Day snowstorm. Wind in ms$^{-1}$ [pennant=25 ms$^{-1}$, full bar=5 ms$^{-1}$], temperature in °C. Heights, surface pressures and isotherms are indicated by solid and dashed lines, respectively. (From Bosart, 1981)

source will be described. Responses to both heating and cooling will be included. The response of a three-dimensional flow to a prescribed local heating will be described and applied to the dynamics of V-shaped cloud tops over severe storms. In Section III, we will review the response of a flow over a meso-$\alpha/\beta$ scale heat source. The effects of planetary rotation will be included in this section. Responses to both barotropic and baroclinic flows will be discussed. The theory will then be applied to the problem of coastal cyclogenesis.

## II. Shear Flow over a Meso-$\gamma$ Scale Heat Source

As discussed in the introduction, diabatic heating in a flow with vertical shear is a common element in various mesoscale circulations (e.g., Lin, 1987). The mathematical problem of adiabatic perturbations to a shear flow in a stably stratified fluid has been studied extensively in the last three decades. Bretherton (1966) found that the vertical wavenumber becomes large and that the group velocity becomes more horizontally oriented as the critical level is approached. Booker and Bretherton (1967) found that the gravity waves are attenuated exponentially as they pass through a critical level at which the horizontal basic wind is equal to the horizontal phase speed if the Richardson number ($Ri$) is everywhere greater than 1/4, i.e., if the flow is dynamically stable. The horizontal momentum is transferred to the basic flow. The critical level problem in an adiabatic flow has been studied by several authors (see Gossard and Hooke, 1975; Maslowe, 1986; LeBlond and Mysak, 1978 for reviews). The response of a stably stratified shear flow with a critical level to a mountain (orographic forcing) has been studied by Smith (1984, 1986). The solutions have been applied to the lee cyclogenesis problem. The response to a diabatic heating has been studied by Lin (1987) and Lin and Chun (1991). The solutions have been used to explain the maintenance of a midlatitude squall line and the formation of density current associated with evaporative cooling.

Observations of large sheared cumulonimbus convection have also suggested that the environmental wind relative to the storm movement often reverses its direction at some height (e.g., Newton, 1966; Marwitz, 1972). In order to understand the effects of latent heating associated with cumulonimbus convection on environmental flow, it is important to study the three-dimensional response of both uniform and sheared stratified flows to diabatic heating. In solving the three-dimensional response to a prescribed elevated heating, representing the latent heating associated with isolated supercell thunderstorms, Lin (1986a,b) and Lin and Li (1988) proposed that the V-shaped cloud tops over severe storms (see Heymsfield and Blackmer, 1988 for a brief review) are formed by the thermally forced gravity waves.

### 1. Two-Dimensional Shear Flow with a Critical Level

The equation governing the two-dimensional steady-state, small-amplitude vertical velocity perturbation in a stratified, nonrotating, Boussinesq fluid with diabatic heating can be simplified from Eq. (15) of Part I (Lin, 1994):

$$U^2 \frac{\partial^2}{\partial x^2}(w'_{xx}+w'_{zz}) - U U_{zz} w'_{xx} + N^2 w'_{xx} = \frac{g}{c_p T_o} q'_{xx}. \tag{1}$$

The homogeneous part of the above equation has been discussed in Bretherton (1966). To simplify the problem, we may assume that the flow is in hydrostatic balance and that the basic wind shear is constant with height. After making the Fourier transform in $x$, the above equation becomes

$$\hat{w}_{zz} + \frac{N^2}{U^2(z)}\hat{w} = \frac{g}{c_p T_o U^2(z)}\hat{q}. \tag{2}$$

In this section, we allow the basic wind to vanish at a certain height. This will introduce a singularity to the equation at the wind reversal level, which coincides with the critical level in a steady state flow. The Brunt-Vaisala frequency, $N$, is assumed to be constant with height, and $U(z)$ is given by

$$U(z) = \alpha z, \quad -H_o \le z, \tag{3}$$

where $\alpha = -U_o/H_o$, $U_o$ is the basic flow at the surface, and $H_o$ is the depth from the surface to the critical level. For convenience, the origin of the vertical coordinate is chosen to be at the critical level. The diabatic heating represents either low-level sensible heating or elevated latent heating, and is assumed to have the form

$$\begin{aligned} q'(x,z) &= Q_o f(x), \quad -H_o \le z < -H_1 \\ &= 0, \qquad -H_1 \le z, \end{aligned} \tag{4}$$

where $H_1$ may be positive or negative, depending upon whether the top of the heating layer is below or above the critical level. Substitution of the Fourier transform of the above equation into Eq. (2) yields

$$\begin{aligned} \hat{w}_{zz} + \left(\frac{N}{\alpha z}\right)^2 \hat{w} &= \frac{g Q_o}{c_p T_o \alpha^2 z^2}\hat{f}(k), \quad -H_o \le z < -H_1 \\ &= 0, \qquad -H_1 \le z. \end{aligned} \tag{5}$$

The general solution of the above equation may be written as

$$\hat{w}(k,z)=A z^{1/2+i\mu}+B z^{1/2-i\mu}+\frac{g Q_o \hat{f}(k)}{c_p T_o N^2},$$

$$-H_o \le z < -H_1$$

$$\hat{w}(k,z)=C z^{1/2+i\mu}+D z^{1/2-i\mu}, \quad -H_1 \le z \qquad (6)$$

where

$$\mu^2 = Ri - 1/4, \quad Ri = N^2/\alpha^2. \qquad (7)$$

The upper radiation condition and lower boundary condition requires $C$=0 (Booker and Bretherton, 1967) and $\hat{w}(z=-H_o)$=0, respectively. The interface conditions at $z=-H_1$ appear to be that both $\hat{w}$ and $\hat{w}_z$ are continuous across it. Applying the boundary and interface conditions to Eq. (6) leads to a solution of $\hat{w}(k, z)$ in Fourier space. A perturbation streamfunction $\psi'$ may be defined as $-\partial\psi'/\partial x=w'$. The vertical displacement ($\eta$) is related to be perturbation streamfunction according to $\eta=-\psi'/U$ if $U\neq 0$. The total streamfunction can then be calculated by

$$\psi=\bar{\psi}+\psi'=\int_{-H_o}^{z} U(z)\,dz+\psi', \qquad (8)$$

or

$$\psi=\left(\frac{U_o H_o}{2}\right)\left[1-\left(\frac{z}{H_o}\right)^2\right]+\psi'. \qquad (9)$$

Using a bell-shaped heating function with compensative cooling, such as that in Eq. (86) of Part I (Lin, 1994), one may obtain solutions in the physical space of the form

$$\psi'=\frac{Q_o}{Ri}\{TNX\{\frac{z1s}{2}[(\cos T1-\cos T2)$$

$$-\frac{1}{2\mu}(\sin T1+\sin T2)]+z0s\cdot\cos T3-1\}$$

$$+LNX\{\frac{z1s}{2}[\frac{1}{2\mu}(\cos T1-\cos T2)$$

$$+(\sin T1+\sin T2)]-z0s\cdot\sin T3\}]$$

$$-1\le z<-H_1 \qquad (10a)$$

$$\psi'=\frac{Q_o}{Ri}\{TNX\{\frac{z1s}{2}[(\cos T1-\cos T2)$$

$$+\frac{1}{2\mu}(\sin T1-\sin T2)]$$

$$-(z1s\cdot\cos T1-z0s\cdot\cos T3)\}$$

$$+LNX\{\frac{z1s}{2}\cdot[\frac{1}{2\mu}(\cos T1-\cos T2)$$

$$-(\sin T1-\sin T2)]+(z1s\cdot\sin T1$$

$$-z0s\cdot\sin T3)\}] \qquad -H_1\le z<0 \qquad (10b)$$

$$\psi'=\frac{Q_o}{Ri}e^{-\pi\mu}[TNX\{\frac{z1s}{2}[\frac{1}{2\mu}(\cos T1-\cos T2)$$

$$-(\sin T1-\sin T2)]+(z1s\cdot\sin T1$$

$$-z0s\cdot\sin T3)\}-LNX\{\frac{z1s}{2}[(\cos T1-\cos T2)$$

$$+\frac{1}{2\mu}(\sin T1-\sin T2)]-(z1s\cdot\cos T1$$

$$-z0s\cdot\cos T3)\}] \qquad 0\le z, \qquad (10c)$$

where

$$z1s=\sqrt{|z|/H_1};\ z0s=\sqrt{|z|};\ T1=\mu\ln(|z|/H_1);$$

$$T2=\mu\ln(H_1|z|);\ T3=\mu\ln|z|;$$

$$TNX=\tan^{-1}x-\tan^{-1}x/b_2;$$

$$LNX=\frac{1}{2}\ln[(b_2^2+x^2)/(1+x^2)].$$

The nondimensional variables are defined by (the tildes are dropped in the above equation)

$$(\tilde{z},\tilde{H}_1)=(z/H_o,H_1/H_o);\ \tilde{\psi}=\psi'/U_oH_o;$$

$$(\tilde{x},\tilde{b}_2)=(x/b_1,b_2/b_1);\ \tilde{Q}_o=Q_o g b_1 H_o/(c_p T_o U_o^3). \qquad (11)$$

The total streamfunction has the nondimensional form

$$\psi=\frac{1}{2}(1-z^2)+\psi'. \qquad (12)$$

Figure 4 shows the total streamfunction and the vertical velocity for a shear flow with $Ri$=10, $H_1$=0.2, and $Q_1$=0.25. Notice that these parameters are nondimensionalized. The corresponding dimensional parameters may be considered as $U_o$=6.3 ms$^{-1}$, $H_o$=2000 m, $H_1$=400 m, and $N$=0.01 s$^{-1}$. The heat source is located below the critical level, $z$=0. The heating depth is 1.6 km. Below the critical level, a broad region of downward displacement is estab-

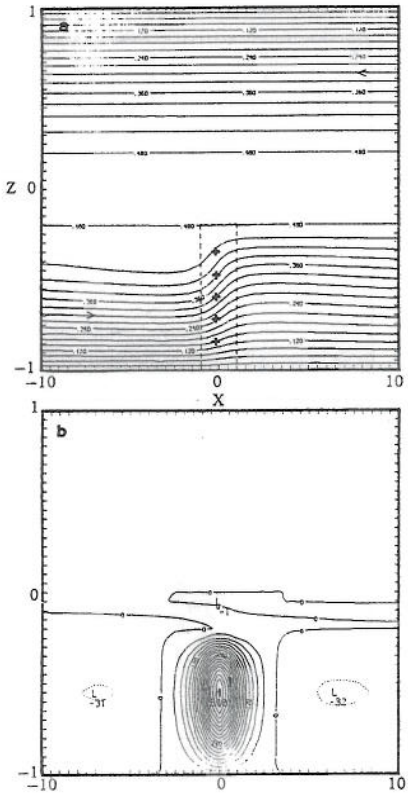


**Fig. 4.** (a) Streamlines for a two-dimensional shear flow with a critical level ($z$=0) over an isolated heat source which is concentrated within the dashed lines. The solution is given by Eq. (10) with $Q_o$=0.25, $Ri$=10, $H_1$=0.2, and $b_2$=10. (b) Vertical velocity for (a). Dashed lines indicate negative vertical velocity. (From Lin, 1987)

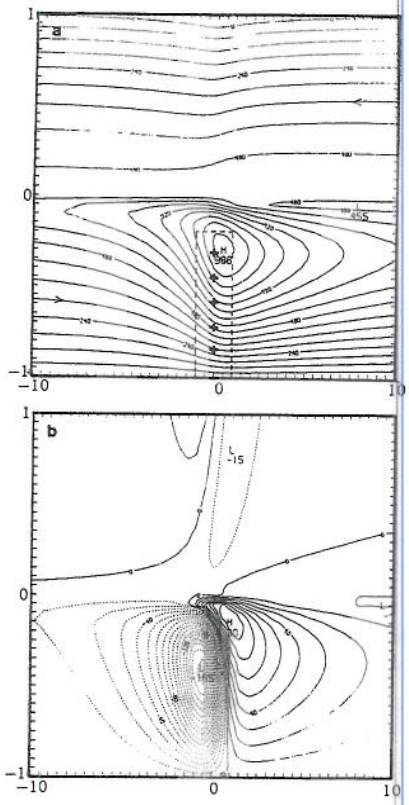


**Fig. 5.** As in Fig. 4 except with $Ri$=1. (From Lin, 1987)

lished upstream of the heat source, followed by a region of upward displacement downstream. The vertical motion is almost symmetric with respect to the heating center because the differential advection effect of the basic wind is small due to the prescribed weak shear. On both the upstream and downstream sides of the updraft, there exist two weak compensated downdrafts. This response is similar to the motions induced in a quiescent stratified fluid (e.g., Lin and Smith, 1986; Nicholls *et al.*, 1991). Above the critical level, the flow is almost undisturbed because the thermally forced gravity waves are attenuated exponentially as they pass through the critical level. This result is consistent with the free wave solution of Booker and Bretherton (1967) and the mountain wave solution of Smith (1986). Beneath the critical level, the local vertical wavelength decreases as the local horizontal basic wind decreases.

Figure 5 shows a case similar to Fig. 4 except with $Ri$=1. The corresponding dimensional parameters may be considered the same as in Fig. 4 except with $U_o$=20 ms$^{-1}$. The response is significantly different from the previous case. The vertical motion is much stronger than the previous case. A region of strong downward motion is established upstream of the heating center. The region of maximum upward motion is shifted downstream of the heating region. The broad descent is produced by the compensating down-draft associated with the updraft. Below the critical level, the region of updraft is displaced downwind. This is caused by the advection effect imposed by the basic wind due to stronger vertical shear, which now exists as compared with previous case. Near the top of the heat source, there exists a region of flow recirculation. The thermally forced gravity wave is able to propagate upward to the upper layer above the critical level although the amplitude is relatively weak. The upstream tilt of the wave in this layer indicates that the wave is able to propagate to infinity. Figure 6 displays the momentum flux for the case of Fig. 5. The momentum flux at the surface is zero as required by the lower boundary condition. The momentum flux has a negative value with increasing magnitude in the heating layer, i.e. -1<$z$<-0.2, and a constant negative value above the heating top until the critical level is reached. This result is consistent with the theory of Eliassen and Palm (1960), which states that the momentum flux does not change with height in a region with no forcing, except possibly at levels where $U$=0. The vertical flux of horizontal momentum increases almost discontinuously to a small positive value above the critical level as the basic flow reverses its direction,

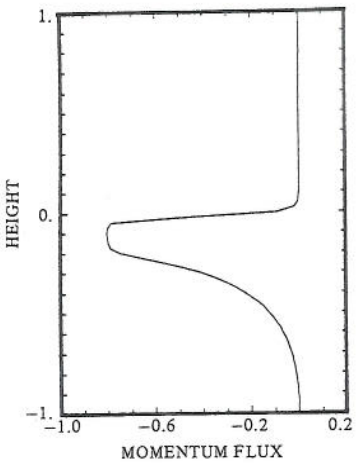


**Fig. 6.** The vertical momentum flux for the flow field of Fig. 5. (From Lin, 1987)

and the disturbance is very weak there. The abrupt increase of the momentum flux across the critical level is associated with the absorption of the wave energy by the critical level. The above solution, Eq. (10), has been adopted by Crook and Moncrieff (1988) in a study on the effect of large-scale convergence on the generation and maintenance of deep moist convection.

Latent heating always exists in the vicinity of the critical level in a moist convection. The procedure for solving the mathematical problem of a shear flow over an elevated heat source which exists in the vicinity of the critical level is similar to the above case (Lin, 1987). Figure 7 shows the response of a shear flow over an elevated heating in a stratified, unbounded fluid. The existence of thermal forcing in the vicinity of the critical level can modify the flow significantly. In the vicinity of the critical level ($z$=0), the fluid particle on the left hand side in the lower layer experiences a strong upward motion near the heating center ($x$=0), crosses the critical level, and then returns to the left of the domain in the upper layer. In addition, the flow near the concentrated heating region is dominated by upward motion, as indicated by Fig. 7b. The consistency of the vertical motion and the heating at the heating base is important in order to support the existing convection (Raymond, 1986). The heating base may represent the cloud base or the top of the moist boundary layer where the surface air becomes unstably buoyant in a cumulus convection (Lindzen, 1974). The vertical motion in the vicinity of the critical level may be explained by inspecting the thermodynamic equation [Eq. (40) of Lin (1994)]:

$$U\frac{\partial \theta'}{\partial x}+\frac{N^2\theta_o}{g}w'=\frac{\theta_o}{c_pT_o}q'. \qquad (13)$$

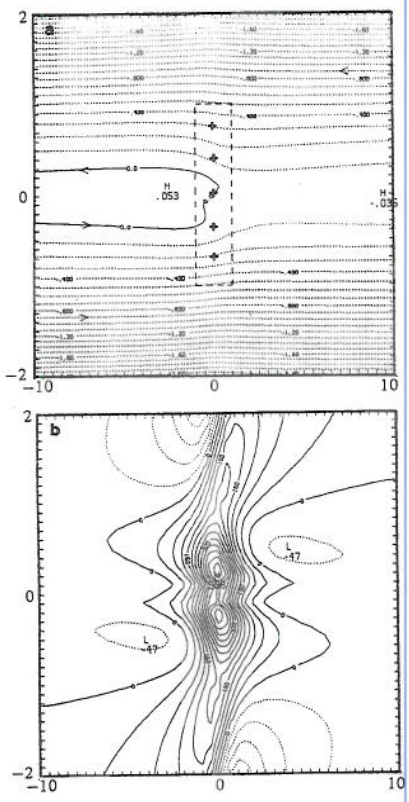


**Fig. 7.** (a) Streamlines for flow over an isolated heat source in an unbounded continuously stratified fluid. The heating is concentrated in the region enclosed by dashed lines. (b) Vertical velocity for (a). The Richardson number associated with the basic flow is 1. (From Lin, 1987)

The above equation may be approximated by

$$w'=\frac{g}{c_pT_oN^2}q' \qquad (14)$$

in the vicinity of the critical level since $U\approx 0$ there. This indicates that the vertical velocity near the critical level is proportional to the heating rate. Since the flow structure resembles that associated with a midlatitude squall line, one may conclude that the condensational heating in the vicinity of the critical level plays an important role in the interaction of the flow below and above the critical level.

Lin and Chun (1991) solved a similar problem analytically for a flow over a low-level heat sink and obtained a result similar to that of Lin (1987). From a scale analysis of the governing equations, a nonlinearity factor of the thermally induced finite amplitude waves, $gQ_ob_1/(c_pT_oU_o^2N)$, is found. The symbol $U_o$ denotes the basic wind at the surface. This factor reduces to that found by Raymond and Rotunno (1989) for the uniform flow case. Using a simple nonlinear model, Lin and Chun (1991) found that the hydrostatic response of a shear flow with a critical level to a steady

cooling can be categorized as either a stationary cold pool, or a density current, depending upon the strength of the effective cooling. For a small Richardson number flow, the cold pool is stationary with respect to the upstream flow because most of the cooling is used to compensate the positive vorticity generated by the positive wind shear (Fig. 8a). In this case, the response is similar to the linear steady state case (Fig. 3a of Lin and Chun, 1991). For a large Richardson number flow, the cold pool is able to propagate upstream because the effective cooling, which increases with time, is strong enough to push the outflow against the basic wind (Fig. 8b). It is interesting to observe that internal gravity waves are produced and propagate upward at the head of the density current. Similar results also were obtained by Chen *et al.* (1992) in a nonhydrostatic numerical simulation of gravity currents. From the comparison between linear theory and nonlinear model results, it is found that the nonlinearity appears to reduce the wave disturbance in the layer between the critical level and the cooling top while it tends to strengthen the density current or cold pool near the surface.

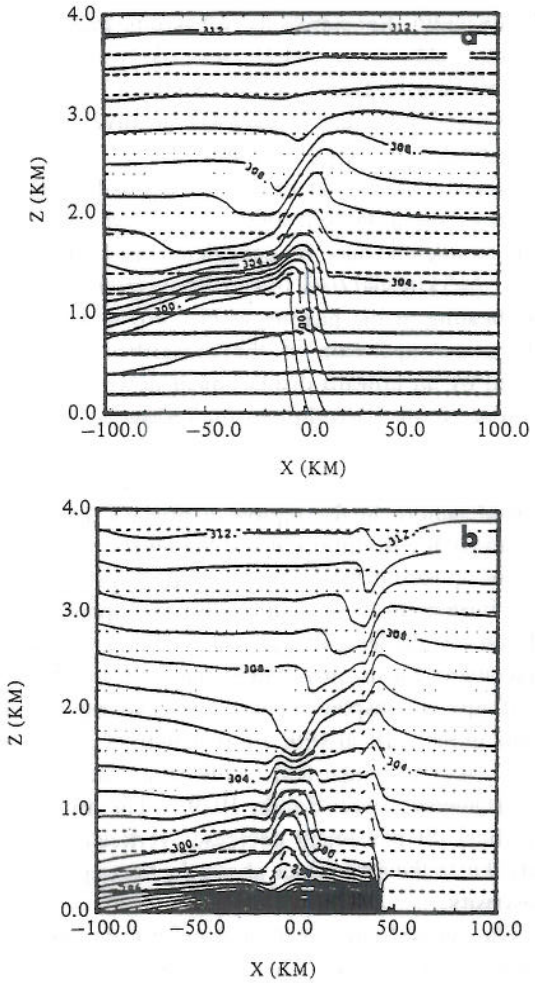


**Fig. 8.** Potential temperature fields for a two-dimensional, hydrostatic, continuously stratified shear flow with a critical level ($z$=2.5 km) over a steady heat sink ($b_1$=10 km, $z$≤1.5 km) for (a) $Ri$=0.69 and $U_o$=30 ms$^{-1}$, (b) $Ri$=6.25 and $U_o$=10 ms$^{-1}$. The basic wind blows from right to left in the lower layer ($z$≤2.5 km) and reverses its direction in the upper layer. Notice that an upstream propagating density current develops in the large Richardson flow. (From Lin and Chun, 1991)

Lindzen and Tung (1976) proposed that a stable wave duct adjacent to the surface may exist if it is capped by an unstable layer which contains a critical level. Chun (1991) has investigated the steady response analytically in the same type of environment but with a diabatic cooling in a three-layer atmosphere. The lower layer adjacent to the surface has a uniform basic wind and serves as a wave duct when the conditions are met. They showed that when the shear layer is dynamically stable ($Ri$≥1/4), almost all of the wave energy is absorbed near the critical level. However, when the shear layer is dynamically unstable, waves can be partially- or over-reflected from the critical level, depending upon the strength of the stability of the shear layer. The wave is almost entirely reflected when $(Ri\text{-}1/4)^{1/2}$ is near 0.4. The transmission coefficient increases as the reflection coefficient increases. In addition, the wave amplitude below the shear layer also depends upon the depth of the lower layer of uniform flow. The wave amplitude in the lower layer becomes maximum when the ratio of the vertical wavelength and the depth of the lower layer is $n/2+1/4$. These factors may modify the vertical motion field significantly, which in turn will either enhance or suppress the new cells produced by the density current.

## 2. Three-Dimensional Flow

Before we discuss the response of a three-dimensional shear flow to elevated heating, it is essential to understand the response of a three-dimensional uniform flow to an elevated heating. Thus, we will review the work of Lin (1986a) first and then the work of Lin and Li (1988). The small amplitude equation governing the vertical velocity for a steady state, three-dimensional, stratified, incompressible, Boussinesq, non-rotating flow can be written as

$$\left(U\frac{\partial}{\partial x}+\nu\right)^2\nabla^2 w'+N^2\nabla_H^2 w'=\left(\frac{g}{c_p T_o}\right)\nabla_H^2 q', \qquad (15)$$

where ν is the coefficient of both Rayleigh friction and Newtonian cooling. To solve the above equation, we determine the relevant Green's function as in previous sections. Taking the double Fourier transform in $x$ and $y$ ($x\rightarrow k$, $y\rightarrow 1$) of the above equation, we have

$$\hat{w}_{zz}+\frac{[N^2-(Uk-i\nu)^2]K^2}{(Uk-i\nu)^2}\hat{w}=\frac{gK^2}{c_p T_o(Uk-i\nu)^2}\hat{q}, \qquad (16)$$

where $K=(k^2+1^2)^{1/2}$ is the horizontal wave number.

Consider a bell-shaped heat source with circular contours:

$$q'(x,y,z)=\frac{Q_o}{(r^2/b^2+1)^{3/2}}\delta(z), \qquad (17)$$

where

$$r=(x^2+y^2)^{1/2}.$$

Taking the double Fourier transform of the above equation and substituting into Eq. (16), we obtain

$$\hat{w}_{zz}+\lambda^2\hat{w}=\frac{g\,Q_o\,b^2K^2e^{-bK}}{2\pi c_p T_o(Uk-iv)^2}\delta(z),\ z\geq -H \qquad (18)$$

where

$$\lambda^2=\frac{[N^2-(Uk-iv)^2]K^2}{(Uk-iv)^2}. \qquad (19)$$

An approximate set of lower and upper boundary conditions are $\hat{w}=0$ at the surface ($z=-H$) and the radiation condition, i.e., $\hat{w}\sim\exp(i\lambda z)$ as $z\to\infty$. At the interface $z=0$, one condition is that $\hat{w}$ is continuous across the interface. Integrating Eq. (18) across the interface yields another condition that $\hat{w}_z$ is continuous. Thus, the solution of Eq. (18) can be obtained:

$$\hat{w}(k,l,z)=\frac{i\,g\,Q_o\,b^2\,K\,e^{-bK}[e^{i\lambda(z+2H)}-e^{i\lambda|z|}]}{4\pi c_p T_o(Uk-iv)[N^2-(Uk-iv)^2]^{1/2}}. \qquad (20)$$

The vertical displacement, $\eta$, defined by $w=U\partial\eta/\partial x$, may be written as

$$\eta(x,y,z)=\int_{-\infty}^{\infty}\frac{gQ_ob^2Ke^{-bK}[e^{i\lambda(z+2H)}-e^{i\lambda|z|}]}{4\pi c_pT_oUk(Uk-iv)\sqrt{N^2-(Uk-iv)^2}}\cdot e^{i(kx+ly)}\,dkdl \qquad z\geq -H. \qquad (21)$$

The above equation may be nondimensionalized by

$$(\tilde{x},\tilde{y})=(x/b,y/b);\ (\tilde{k},\tilde{l},\tilde{K})=(bk,bl,bK);$$

$$\tilde{v}=vb/U;\ (\tilde{\eta},\tilde{z},\tilde{H})=(\eta N/U,zN/U,HN/U);$$

$$\tilde{Q}_o=Q_o\,g\,b/(c_p T_o U^3) \qquad (22)$$

to yield

$$\eta(x,y,z)=\int_{-\infty}^{\infty}\frac{\hat{q}(K)K[e^{i\lambda(z+2H)}-e^{i\lambda|z|}]}{2k(k-iv)\sqrt{1-M^2(k-iv)^2}}\cdot e^{i(kx+ly)}\,dkdl, \qquad (23)$$

where

$$\hat{q}(K)=\frac{Q_o}{2\pi}e^{-K}.$$

Notice that the nonhydrostatic effect is represented by a nondimensional number $M$ ($=U/bN$), which is proportional to the ratio of the period of a buoyancy oscillation ($2\pi/N$) to the time it takes for an air parcel to pass the heat source ($b/U$). This reasoning is similar to the mountain wave problem in which the horizontal scale is measured by the mountain width. For simplicity, we assume that the flow is hydrostatic ($M\ll 1$) in most cases. A two-dimensional FFT (Fast Fourier Transform, see Smith, 1979 for a brief review) algorithm can be employed to invert the above solution back to the physical space.

Figure 9 shows an example of a hydrostatic flow ($M=0$) over a shallow heat source with $\tilde{H}=\pi$. The dimensional parameters may be considered as $U=10$ ms$^{-1}$, $N=0.01$s$^{-1}$, $b=5$ km, and $H=3.14$ km. The response of the fluid to the heating at the heating level ($z=0$) is a downward displacement upstream of the prescribed heat source followed by an upward displacement downstream. This is similar to the two-dimensional flow as studied in earlier sections. The region of disturbance widens in general as one moves aloft and beneath the heating level. A V-shaped pattern in the region of upward displacement forms above the heating center at the level of $z=\pi/2$. This region of upward displacement is shifted upstream as one moves further aloft as required by the upper radiation condition. At the level of $z=\pi$, a new region of downward displacement forms just downstream of the V-shaped area of upward displacement. The response is almost periodic in the vertical with a wavelength of $\pi$ (e.g., comparing Figs. 9a, c) like that in the hydrostatic mountain waves (Queney, 1947; Smith, 1979). The amplitude of the vertical dis-placement decreases vertically, which is mainly due to the divergence above the heating region and the viscosity.

The vertical cross section at $y=0$ for the above case is plotted in Fig. 10a. The upstream phase tilt of the disturbance above the heating level ($z=0$) indicates that the wave energy is able to propagate upward (Eliassen and Palm, 1960). The term $\exp(i\lambda(z+2H))$ in the numerator of Eq. (23) represents the reflected waves from the surface, which may cancel the direct upgoing wave, i.e., the term $\exp(i\lambda|z|)$, above the heating level with certain values of $H$. This is similar to the two-dimensional flow (Smith and

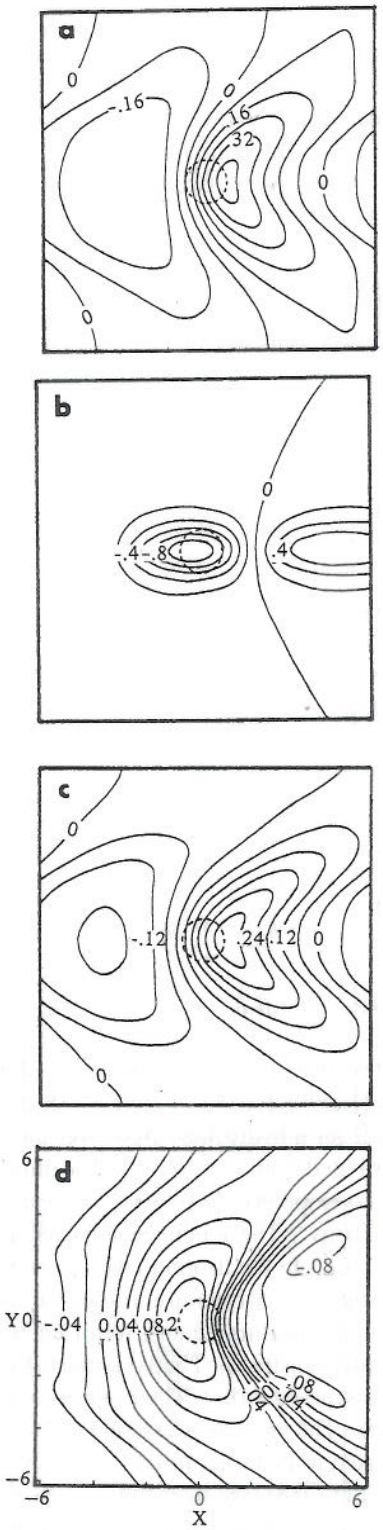


Fig. 9. Vertical displacement of a three-dimensional, continuously stratified, hydrostatic, uniform flow over an isolated heat source which is added at $z$=0. The dashed circle is the heating contour at $r$=$b$. The basic flow is directed from left to right in the positive $x$ direction. The solution is given by Eq. (23) with $H$=$\pi$, $M$=0, $\nu$=0.2. The four levels shown are: (a) $-\pi/2$, (b) 0, (c) $\pi/2$, and (d)$\pi$. (From Lin, 1986a)

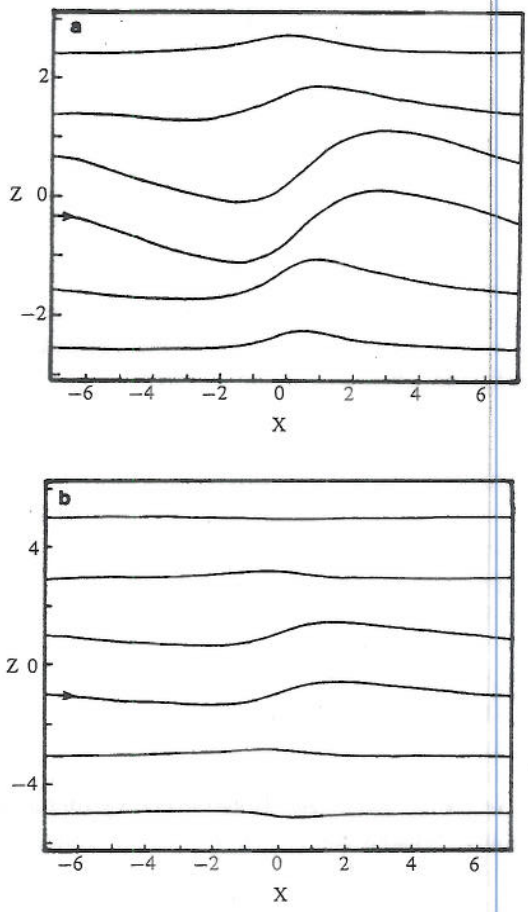


Fig. 10. (a) Vertical cross section along $y$=0 for Fig. 9 ($H$=$\pi$), (b) as in (a) except $H$=$2\pi$. (From Lin, 1986a)

Lin, 1982). One example with $H=2\pi$ is shown in Fig. 10b, in which the disturbance above the heating level ($z$=0) is much weaker than the case of Fig. 10a.

The formation of the V-shaped pattern of the vertical displacement can be explained by the group velocity argument (Lin and Li, 1988). The dispersion relation for an internal gravity waves in a stagnant Boussinesq fluid is

$$\omega=\pm\left[\frac{N^2(k^2+l^2)}{k^2+l^2+m^2}\right]^{1/2}, \tag{24}$$

where $\omega$ and $m$ are the frequency and the vertical wave number, respectively. The group velocity can then be found:

$$c_{gx}=-\frac{\partial\omega}{\partial k}=\frac{-Nkm^2}{[k^2+l^2]^{1/2}[k^2+l^2+m^2]^{3/2}}, \tag{25a}$$

$$c_{gy}=-\frac{\partial\omega}{\partial l}=\frac{-Nlm^2}{[k^2+l^2]^{1/2}[k^2+l^2+m^2]^{3/2}}, \tag{25b}$$

The vertical velocity can be obtained immediately from the dimensional relationship $w'=U\partial\eta/\partial x$ for a steady flow. Figure 12 shows the vertical velocities at the heating base $z_1$ for $(z_1, z_2)$ = (2, 18), (1, 9), (0.5, 4.5), (0.25, 2.25), and (0.125, 1.125). The dimensional parameters may be considered as $N$=0.01 $s^{-1}$, $z_1$=1 km, $z_2$=9 km, $b$=5 km, and $U$=5, 10, 20, 40, 80 $ms^{-1}$. For a fixed heating depth (dimensional), a smaller $z_2-z_1$ corresponds to a higher basic wind speed. Figure 12b corresponds to the case of Fig. 11. The advection effect is more significant for cases with larger basic winds, which give a more pronounced V-shaped pattern. This figure indicates that an upward motion at the cloud base as required by a wave-CISK mechanism may be satisfied with a wide variety of basic wind speeds in the present model, although the air still has to overcome the downward displacement established upstream of the heating region, as pointed out by Raymond (1986).

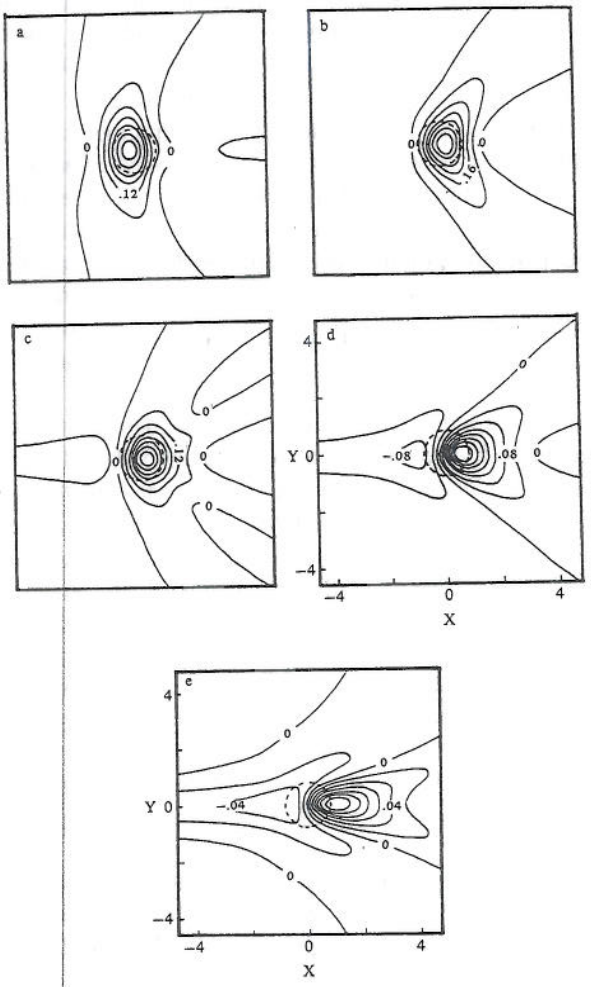


**Fig. 12.** Vertical velocity at $z=z_1$ of a three-dimensional, continuously stratified, hydrostatic, uniform flow over a heat source which is uniformly distributed from $z_1$ to $z_2$. The solution is given by Eq. (31) with $M$=0 and $\nu$=0.2. The four cases of different $(z_1, z_2)$ shown are: (a) (2, 18), (b) (1, 9), (c) (0.5, 4.5), (d) (0.25, 2.25), and (e) (0.125, 1.125). (From Lin, 1986a)

In a study of three-dimensional inviscid airflow over an isolated mountain, Smolarkiewicz and Rotunno (1989) found that a pair of vortices form on the lee side of the mountain in a low Froude number ($Fr=U/Nh<0.5$) flow. The formation of these lee vortices is explained by the tilting of horizontal vorticity produced baroclinically in an inviscid continuously stratified fluid. Smith (1989) commented that the lee vortices can be generated by either a density surface interaction or by overturning and turbulence in an inviscid fluid. It is suspected here that a similar phenomenon may occur in an inviscid flow over a heating source or sink. However, this hypothesis remains to be tested. A nonlinear model is needed to examine the possibility of the formation of vortices on the lee of a heat source or sink. With the Coriolis force included in a study similar to that of Smolarkiewicz and Rotunno (1989), Lin *et al.* (1992) demonstrated that a lee mesocyclone can be generated in a three-dimensional, inviscid, low Froude number flow past an isolated mountain. A similar analogy may be drawn for a flow over a meso-$\beta/\alpha$ scale heat source or sink. If a mesocyclone forms, it may be related to the formation of coastal cyclones. Again, this remains to be investigated in further studies.

The theory developed above may be extended to include a multi-directional shear flow with a critical level. The governing equation is a combination of Eqs. (1) and (15):

$$\left(U\frac{\partial}{\partial x}+V\frac{\partial}{\partial y}+\nu\right)^2\nabla^2 w'-\left(U\frac{\partial}{\partial x}+V\frac{\partial}{\partial y}+\nu\right)$$

$$\cdot\left(U_{zz}\frac{\partial}{\partial x}+V_{zz}\frac{\partial}{\partial y}\right)w'+N^2\nabla_H^2 w'=\frac{g}{c_p T_o}\nabla_H^2 q' \qquad (32)$$

After making the double Fourier transform in $x$ ($\rightarrow k$) and $y$ ($\rightarrow l$), the above equation becomes

$$\hat{w}_{zz}+\left\{\frac{-(kU_{zz}+lV_{zz})}{kU+lV-i\nu}+\left(\frac{N^2}{(kU+lV-i\nu)^2}-1\right)K^2\right\}\hat{w}$$

$$=\frac{gK^2}{c_p T_o(kU+lV-i\nu)^2}\hat{q}(k,l,z). \qquad (33)$$

Again, the heating can be assumed to be a bell-shaped function in $x$ and $y$ and to be uniformly distributed in the vertical. The mathematical problem is complicated. Thus, a simple numerical technique may be adopted to obtain the solution which can provide a physical solution to the problem. Equation (33) in the Fourier space is a special case of the general form of the Taylor-Goldstein equation

$$\zeta_{zz}+p(z)\,\zeta=r(z) \qquad (34)$$

with the boundary conditions

$$\zeta(z_o) = \zeta_o \quad \text{at } z = z_o$$

$$\zeta(z_T) = \zeta_T \quad \text{at } z = z_T, \tag{35}$$

where the subscripts $o$ and $T$ represent the lower and upper boundaries, respectively. Applying a center-difference numerical scheme to the above equation yields

$$(-2\zeta_1 + \zeta_2) + h^2 p_1 \zeta_1 = h^2 r_1 - \zeta_o$$

$$(\zeta_{i-1} - 2\zeta_i + \zeta_{i+1}) + h^2 p_i \zeta_i = h^2 r_i, \quad i = 2, 3, \ldots, n-1$$

$$(\zeta_{n-1} - 2\zeta_n) + h^2 p_n \zeta_n = h^2 r_n - \zeta_T, \tag{36}$$

where $h$ is the interval for numerical integration. In the following examples, the $h$ and horizontal grid interval are chosen to be 250 and 1500 m, respectively. The above linear system can be solved by applying the Gaussian elimination scheme to the banded matrix column vector $[\zeta_1, \ldots, \zeta_n]$ as long as the boundary conditions are known. The upper radiation boundary condition is simulated by a sponge layer (Klemp and Lilly, 1978), in which the coefficient of Rayleigh friction and Newtonian cooling is gradually increased by a factor of 5 in the sponge layer according to a sine square function. Once the numerical solution in the Fourier space is obtained, a two-dimensional FFT algorithm can be adopted to invert the solution back to the physical space.

Figure 13 shows the flow fields for a nonhydrostatic shear flow over an elevated heat source. A linear shear, $U(z)=-U_o+(U_o/z_c)z$ and $V(z)=0$, is assumed in this case. The critical level ($z_c$) is located at 2 km. Other parameters chosen are: $N=0.01\ s^{-1}$, $U_o=10\ ms^{-1}$, $Q_o=4\ J\,kgs^{-1}$, $b=5$ km, $z_1=1.5$ km, $z_2=12$ km, and $\nu=10^{-4}\ s^{-1}$. A rather small heating rate is used to avoid the violation of the small amplitude assumption. The cloud base and top can be assumed to be 1 km and 14 km, respectively. Even though these values are not involved in the calculation, it should be noted that the cloud base and top are not necessarily located exactly at the same height as the heating base and top, respectively. The Richardson number associated with the basic flow is 4. The grid resolution is 64×64×101. The actual horizontal domain is 94.5 km×94.5 km. Only the central portion, 46.5 km×46.5 km, are shown in the figure. The horizontal domain is chosen to be large enough so that the effect of periodic conditions assumed by the FFT algorithm can be minimized. The vertical extent of the physical layer is 15 km while the sponge layer extends from 15 km to 25 km.

At the cloud base ($z$=1 km), the basic wind blows from right to left. Upward motion is generated upstream of the heating center with downward motion downstream of the heating. The region of upward motion forms a V-shaped pattern with the vertex pointing upstream. The V-shaped pattern of upward velocity in the low levels has also been found in numerical simulations (e.g., Klemp and Wilhelmson, 1978; Schlesinger, 1980). The formation of this V-shaped pattern is similar to that discussed in the last section except with downward propagating gravity waves. Evidence of these downward propagating waves is also shown in the upstream shift of the maximum updraft from Figs. 13a, b and f. At the heating base $z_1$ (Fig. 13b), the heating region is dominated by upward motion. The colocation of the upward motion and the heating at the heating base is important in supporting the existing convection. Moving further aloft to the critical level, $z_c$=2km, the response of the airflow to the diabatic heating is an axisymmetric region of upward motion (Fig. 13c). Similar to the two-dimensional case (Eq. (14)), the vertical velocity at the critical level is directly proportional to the heating according to the thermodynamic equation since the basic wind vanishes there. Thus, the region of upward motion reproduces the bell-shaped pattern of the heat source. Notice that the basic wind profile used in this case agrees better with squall lines and multicell storms than with right or left moving supercells, which would maintain a constant storm-relative V-component $V(z)=\pm V_o$ to the wind. The gravity wave pattern produced by this type of supercell has been better represented in Lin (1986a) and Raymond (1986). The positive response of vertical motion at the cloud base depends upon the heating-induced Froude number $[F=U/N(z_2-z_1)]$, which corresponds to the wave-CISK modes (Raymond, 1986). At higher levels, such as 5 and 14 km (Figs. 13d and e), the V-shaped regions of upward motion are pronounced. This result is consistent with the non-sheared case studied by Lin (1986a) and with numerical modeling studied by Klemp and Wilhelmson (1978) and Schlesinger (1988). The vertical motion is weaker at 14 m than at lower levels because of the divergence above the heating region and the viscosity. Due to the nonhydrostatic effect, repeated, damped oscillations of the disturbance may be produced (e.g., Fig. 2e of Lin and Li, 1988). The formation of V-shaped patterns of vertical velocity was explained earlier by Eq. (30).

The vertical cross section of vertical velocity along $y$=0 is shown in Fig. 13f. In the concentrated heating region, the vertical velocity is positive in the heating layer, with a maximum located at about 5.5 km. The vertical orientation of the updraft core depends on the vertical shear of the environmental wind. The slight downshear tilt is due to the strong advection of the basic wind. For a relatively weak shear case, the updraft is almost vertical. The upstream tilt of the vertical velocity above the heating top (12 km) is offset by the advection effect (Fig. 13f). The downward motion on the downshear side (right side in Fig. 13f) of the updraft is evidence for the existence of the thermally forced gravity wave. Below the cloud base (1 km), the updraft is shifted upstream, followed by a downdraft region. This sloping

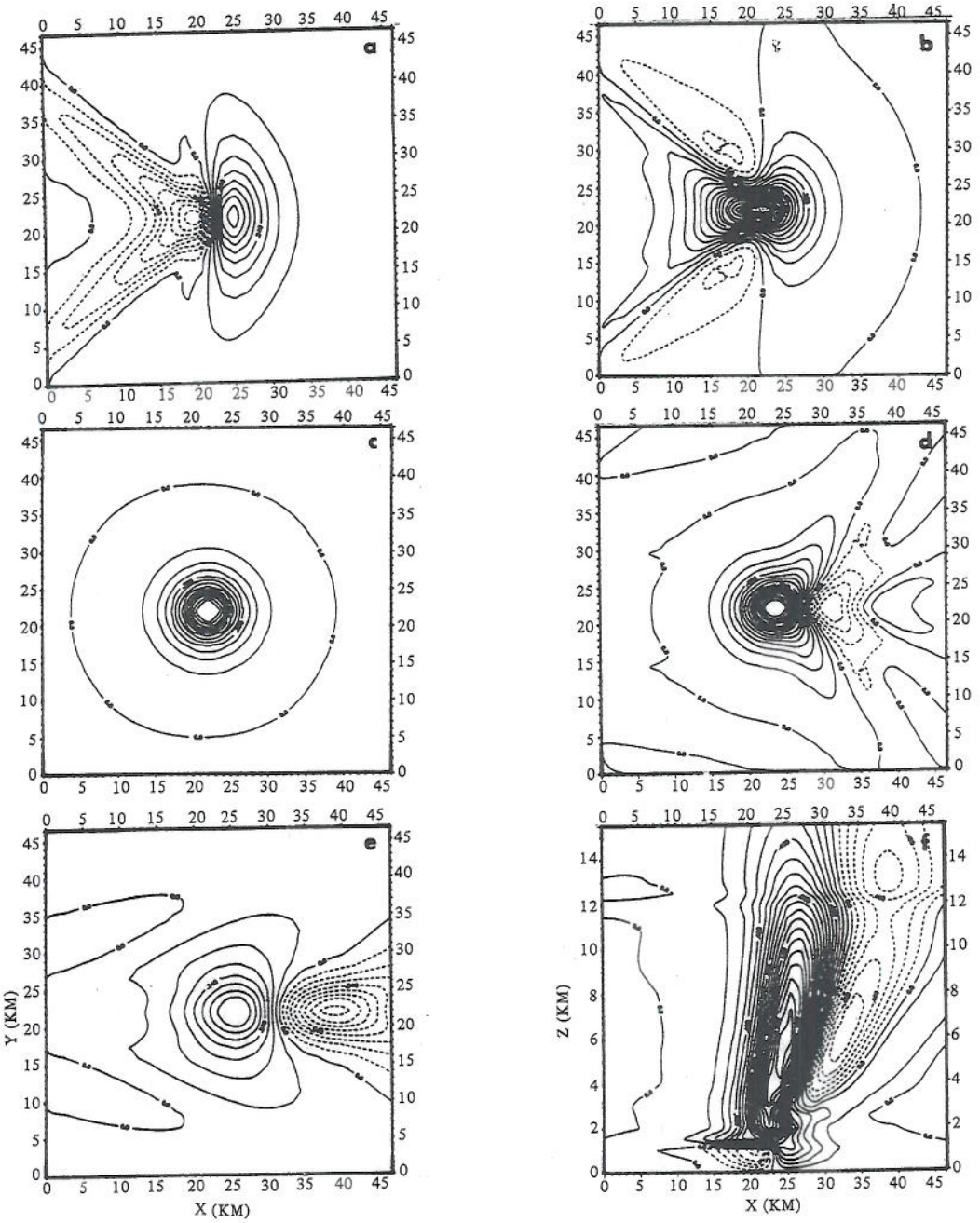


**Fig. 13.** Vertical velocity fields for a nonhydrostatic continuously stratified shear flow over an elevated heat source. The critical level ($z_c$) is located at 2 km. The solution is given by Eq. (23) and solved by the numerical scheme Eq. (36) and an FFT algorithm. Other parameters chosen are: $N$=0.01 $s^{-1}$, $U_o$=10 $ms^{-1}$, $Q_o$=4 J $kgs^{-1}$, $b$=5 km, $z_1$=1.5 km, $z_2$=12 km, and $\nu$=$10^{-4}$ $s^{-1}$. The Richardson number associated with the basic flow is 4. Five levels are shown for: (a) 1 km, (b) 1.5 km ($z_1$), (c) 2 km ($z_c$), (d) 5 km, and (e) 14 km. The vertical cross section along $y$=0 is shown in (f). Units for the vertical velocity are in $ms^{-1}$. (From Lin and Li, 1988)

updraft near the cloud base may enhance the formation of new convective cells. These new convective cells may develop to be part of the supercell or as a short-lived cell in a long-lived convective system (Rotunno *et al.*, 1988).

The propagation of wave energy induced by a stationary heat source in an unbounded, steady stratified shear flow is sketched in Fig. 14. At upper levels, the energy propagates upward and upstream relative to the air ($c_{ga}$) but is advected downstream by the basic wind. Thus, the wave energy is found to be along the direction of $c_{gh+}$ or $c_{gh-}$ relative to the heat source. The formation of the repeated, damped oscillations of the disturbance (Fig. 13f) is mainly due to the nonhydrostatic effect. Similar to mountain wave theory (Smith, 1979), this nonhydrostatic wave only occurs when the dominant squared wave number ($K^2$) is less than the Scorer parameter ($N^2/U^2(z)$) for a Boussinesq, constant

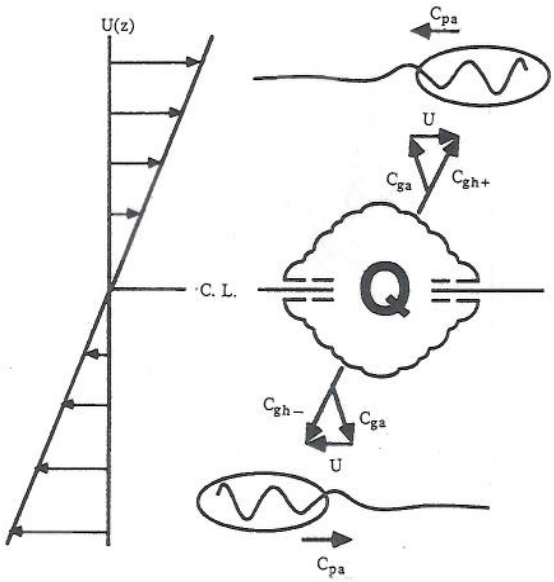


**Fig. 14.** A sketch for the propagation of wave energy associated with steady waves forced by a prescribed heating in an unbounded, nonhydrostatic continuously stratified shear flow. Symbols $c_{pa}$, $c_{ga}$, $c_{gh+}$, and $c_{gh-}$ represent the phase velocity with respect to (w.r.t.) the air, group velocity w.r.t. the air, upward group velocity w.r.t the heat source, and downward group velocity w.r.t. the heat source. (From Lin and Li, 1988)

shear flow. This result also can be explained by the group velocity argument. For simplicity, let us consider a corresponding two-dimensional flow for which Eq. (28a) reduces to

$$\frac{z}{x}=\left(\frac{N}{U}\right)\frac{(1-k^2U^2/N^2)^{1/2}}{k}. \tag{37}$$

The wave energy propagates along the straight line given by the above equation, emanating from the origin where the heat source is located. Now it becomes clear that, in order to have the wave energy propagate downstream ($x>0$) and upward ($z>0$), it is required that $K^2<N^2/U^2(z)$. To determine the control parameter of the downstream wavelength of the heating-induced gravity wave, we assume that the wavelength at a certain height, $z^*$, above the critical level (denoted by C.L. in Fig. 14) is $L$. Thus, $x^*$, $k^*$, and $U(z)$ are equal to $L$, $2\pi/L$ and $U_z z$, respectively. Substituting $z^*$, $x^*$, and $k^*$ into Eq. (37) and solving for $L$, we obtain

$$L=\frac{\sqrt{2}\,\pi z}{Ri^{1/2}}\left[1\pm\sqrt{(1+Ri/\pi^2)}\,\right]^{1/2}.$$

Thus, the downstream wavelength is approximately proportional to $Ri^{-1/2}$ for a stable flow with a relatively strong shear ($Ri<<\pi^2$). A rough estimate from Fig. 13f gives $L$=34 km for $Ri$=4. This result is consistent with the above conclusion.

Figure 15 shows a case with a multi-directional shear. The hodograph is depicted in Fig. 15e. At the cloud base, 1 km, the basic wind blows from the southeast (Fig. 15a). The regions of upward and downward motion are located on the upwind and downwind sides, respectively. The extrema of the vertical velocity are lined up along the direction of the basic environmental wind. The vertical velocity field shows an asymmetric pattern, which is caused by weak advection of gravity waves by the north-south component of the basic wind. This asymmetry is also shown in the field of vertical displacement (Fig. 15b). In the vicinity of the heating region, the flow is dominated by an upward displacement. The downward displacements on the upstream (southeast) and downstream (northwest) sides are relatively small compared with the upward displacement. Even though the north-south wind is relatively weak at the cloud top level (14 km), asymmetric patterns are still pronounced in the fields of vertical velocity and displacement (Figs. 15c and d). Thus, the thermally forced gravity waves in a multi-directional shear help to explain (Heymsfield *et al.*, 1983a; Lin and Li, 1988) the asymmetric pattern of V-shaped cloud tops, such as those observed by Anderson (1982).

## III. Three-Dimensional Flow over a Meso-$\alpha/\beta$ Heat Source

For a stably stratified flow over a diabatic heat source or sink with a horizontal scale on the order of one hundred kilometers, the rotational effect plays an important role in generating inertia-gravity waves. Those waves behave differently from pure gravity waves which are generated by a heat source or sink with a horizontal scale on the order of ten kilometers or smaller. They are also different from quasi- geostrophic planetary waves which are generated by a heat source or sink with a horizontal scale on the order of one thousand kilometers. In this type of flow, the $\beta$-effect may be neglected, but the inertial effects should be included.

By prescribing an isolated diabatic heat source/sink, Rotunno (1983) has investigated the rotational effects on the land and sea breeze circulation in an uniform flow theoretically. Using a similar approach, Hsu (1987a) has studied the two-dimensional nonrotating uniform flow response to a prescribed, finite surface heating with Fickian thermal diffusion included. The horizontal scale of the heating varies from 1 to 1000 km. This work was extended numerically to include three-dimensionality and applied to the snowstorm problem of Lake Michigan (Hsu, 1987b). Some interesting results have been found by Hsu by varying the shape of the diabatic heating and the basic wind directions. However, the energy propagation of the heating-induced inertia-gravity waves has not been emphasized

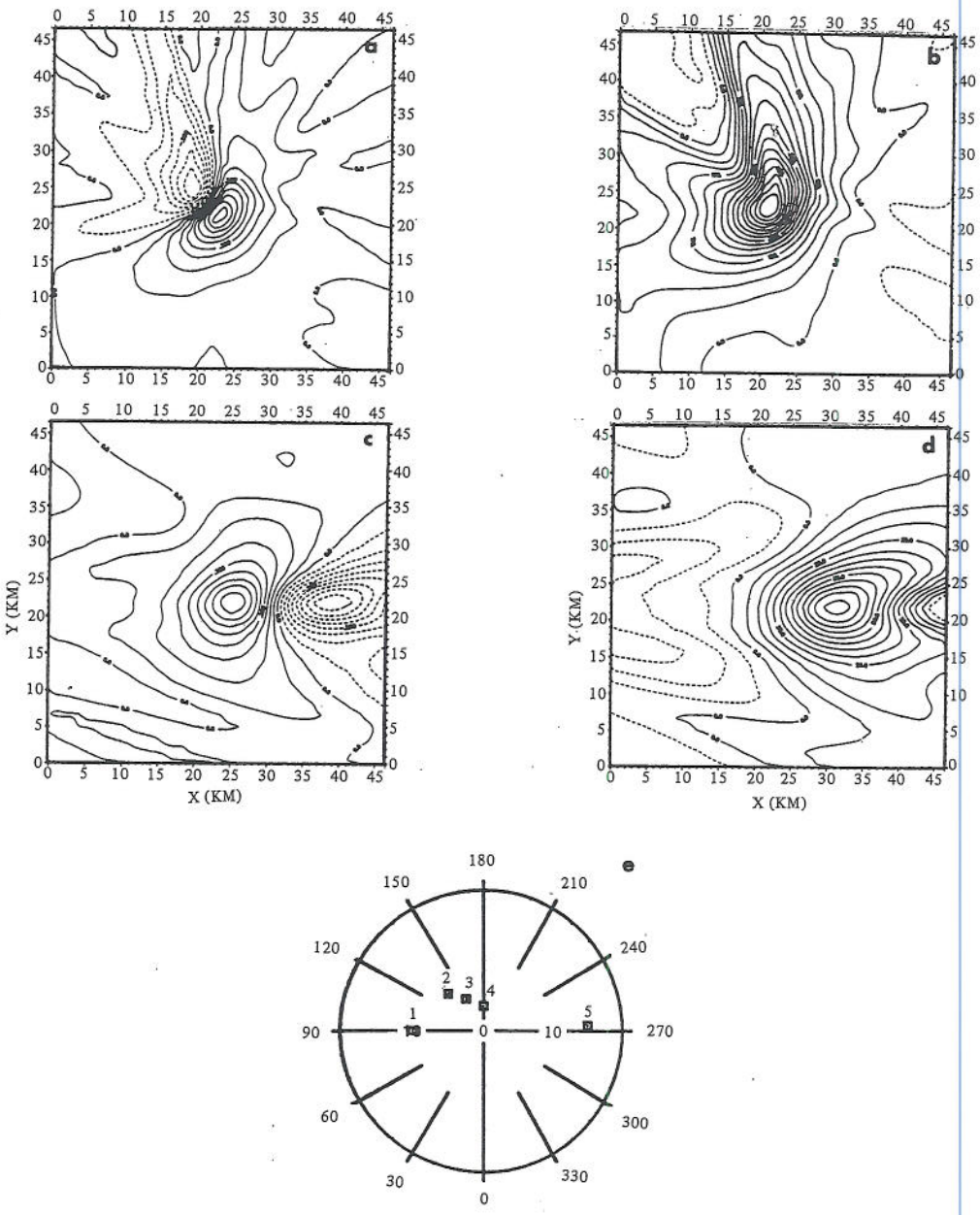


**Fig. 15.** As in Fig. 13 except with a multidirectional shear as sketched in the hodograph (e). Fields plotted are: (a) $w'$ at 1 km (cloud base), (b) $\eta$ at 1 km, (c) $w'$ at 14 km (cloud top), and (d) $\eta$ at 14 km. (From Lin and Li, 1988)

and needs to be investigated for a better understanding of the dynamics. Using a linear theoretical model, Luthi *et al.* (1989) studied the nature and the flow response to prescribed low-level, mesoscale steady state diabatic heating with Rossby numbers greater and smaller than 1. They found that the response is strongly sensitive to: the horizontal scale of the diabatic region, the three-dimensional effects, basic rotation of the flow system and the strength of the momentum and thermal damping. The inertial effects of a three-dimensional uniform flow over a mesoscale heat source have been investigated by Lin (1989a) by comparing the response with that of a quasi-geostrophic flow. This work will be reviewed in this section.

The above problem is related to the shear flow over the East Coast of the United States. Cyclogenesis along the east coast of the United States has received considerable attention since the recent completion of the Genesis of Atlantic Lows Experiment (GALE). These cyclones often form off the Carolina coast, develop rapidly, and move northeastward, which may bring heavy snowfall and damage over the mid-Atlantic states. Different kinds of approaches, such as observational data analysis (e.g., Bosart, 1981; Uccellini *et*

*al.*, 1984), numerical simulations (e.g., Anthes *et al.*, 1983; Orlanski and Katzfey, 1987) and theoretical studies (e.g., Smith, 1986; Lin, 1989b, 1990a), have been used to investigate the problem of East Coast cyclogenesis. Observational studies suggest that there are two major mechanisms responsible for the East Coast cyclogenesis. The first may be called the boundary-layer control of cyclogenesis (e.g., Bosart, 1981, 1988). It is proposed that the cyclonically curved coastline under a northeasterly flow is favorable for the growth of cyclonic vorticity in response to differential heating and differential friction between a relatively warm ocean and colder landmasses. The second mechanism may be called the upper-level jet streak/trough control of cyclogenesis (e.g., Uccellini *et al.*, 1984; Uccellini and Kocin, 1987). It is proposed that the circulation patterns associated with jet streaks establish an environment within which low-level processes can further contribute to cyclogenesis. The transverse ageostrophic components associated with jet streaks aloft combine with the longitudinal components associated with trough-ridge systems and can provide for the upper-level divergence conducive to surface cyclogenesis as envisioned by Bjerknes (1951). It appears that the boundary-layer mechanism is more responsible for the early formation of the coastal cyclone while the upper-level forcing mechanism is more responsible for the later development. One example is the case of GALE IOP#2 (GALE, 1986), in which there are no migratory shortwave trough/jet streaks aloft to account for the cyclogenesis at the early stage. As a shortwave trough aloft moves over the genesis region at a later time, the cyclone begins to move northeastward and develops further along the coastal front. In order to understand the effect of differential heating on the development of a coastal cyclone, it is important to study the response of a baroclinic flow to a low-level heating. In this paper, we will review the responses of a baroclinic flow over a prescribed low-level heat source studied by Lin (1989b, 1990a) and some recent results.

In order to help understand the basic dynamics of the responses in a rotating shear (baroclinic) flow, we will review the responses in a rotating uniform (barotropic) flow first.

## 1. Steady Barotropic Flow

The small-amplitude equation of vertical velocity for a steady, three-dimensional, stratified, hydrostatic Boussinesq flow in a rotating system may be written as

$$U u'_x - f v' = -(1/\rho_o) p'_x \tag{38}$$

$$U v'_x + f u' = -(1/\rho_o) p'_y \tag{39}$$

$$p'_z = (g\rho_o/\theta_o)\theta' \tag{40}$$

$$u'_x + v'_y + w'_z = 0 \tag{41}$$

$$U\theta'_x + (\theta_o N^2/g) w' = (\theta_o/c_p T_o) q'. \tag{42}$$

The above equations may be nondimensionalized by

$$(\tilde{x},\tilde{y}) = (x/b, y/b);\ \tilde{z} = z/H_o;$$

$$(\tilde{u},\tilde{v}) = (u'/U, v'/U);$$

$$\tilde{w} = w' b/(R_o U H_o);\ \tilde{p} = p'/(\rho_o f U b);$$

$$\tilde{\theta} = (\theta' g H_o)/(f\theta_o U b);$$

$$\tilde{q} = q' g H_o/(c_p T_o U^2 f), \tag{43}$$

to yield (with tildes dropped)

$$R_o u_x - v + p_x = 0 \tag{44}$$

$$R_o v_x + u + p_y = 0 \tag{45}$$

$$p_z - \theta = 0 \tag{46}$$

$$u_x + v_y + R_o w_z = 0 \tag{47}$$

$$\theta_x + w = q, \tag{48}$$

where $b$ is the horizontal scale of the heat source, and $R_o = U/fb$ and $H_o = fb/N$ are the Rossby number and the deformation depth (e.g. see Buzzi and Tibaldi, 1977; Pierrehumbert and Wyman, 1985).

To investigate the inertial effects, we will consider the flow response in a quasi-geostrophic system. This will provide a basis for comparison. Equations (44)-(48) can be reduced to a single equation for the pressure perturbation by making the quasi-geostrophic approximation, i.e., by retaining the zeroth and first order terms in a Taylor series expansion of the dynamical variables in powers of $R_o$ (for details, see Pedlosky, 1982):

$$\frac{\partial}{\partial x}(p_{zz} + \nabla_H^2 p) = q_z. \tag{49}$$

The lower boundary, with Ekman friction (Charney and Eliassen, 1949) included, requires

$$w' = -\left(\frac{U}{\rho_o N^2}\right) p'_{xz} + \left(\frac{g}{c_p T_o N^2}\right) q' = H_o\left(\frac{1}{2} E^{1/2}\right)\zeta'$$

$$\text{at } z = 0, \tag{50}$$

where $E = \nu/(fH_o^2)$ is the Ekman number, and $\zeta'$ is the vertical component of the relative vorticity. The nondimensional form of the above equation is

$$p_{xz} + [(E^{1/2}/2)/R_o]\zeta = q \quad \text{at } z = 0. \tag{51}$$

For a low-level thermal forcing, we may assume

$$q'(x,y,z) = h'(x,y)\, e^{-z/H_1}, \tag{52}$$

where $h'(x,y)$ is the horizontal distribution of the heating, and $H_1$ is the e-folding depth of the heating. The above equation can be expressed in nondimensional form:

$$q(x, y, z) = h(x, y)\, e^{-z/\gamma}, \tag{53}$$

where $\gamma = H_1/H_o = NH_1/fb$ is the aspect ratio of the heating depth to the deformation depth.

To solve the problem, we make the double Fourier transform in $x$ and $y$ of Eqs. (49), (51), and (53):

$$\hat{p}_{zz} - K^2 \hat{p} = -\left(\frac{\hat{h}}{i\gamma k}\right) e^{-z/\gamma}, \tag{54}$$

with

$$\hat{p}_z - \left\{\frac{(1/2)E^{1/2}K^2}{R_o\, ik}\right\}\hat{p} = \frac{\hat{h}(k,l)\, e^{-z/\gamma}}{ik} \quad \text{at } z = 0. \tag{55}$$

The general solution of Eq. (54) can be written as

$$\hat{p} = Ae^{-Kz} + Be^{Kz} - \frac{\hat{h}\,\gamma e^{-z/\gamma}}{ik(1-\gamma^2 K^2)}. \tag{56}$$

The upper boundary condition requires $p \to 0$, which implies $B=0$. After applying the lower boundary condition (55), the solution in the Fourier space can be obtained:

$$\hat{p} = \frac{\hat{h}\,\gamma}{ik(1-\gamma^2K^2)}\left\{K\left[\gamma + \frac{(E^{1/2}/2)(1-\gamma K)}{R_o\, ik + (E^{1/2}/2)K}\right]\right.$$

$$\left. \cdot\, e^{-Kz} - e^{-z/\gamma}\right\}. \tag{57}$$

Other variables are related to $p$ by the following relationships:

$$w = -p_{xz} + q, \quad u = -p_y, \quad v = p_x,$$

$$\zeta = \nabla_H^2 p, \quad \delta = R_o(p_{xzz} - q_z), \tag{58}$$

where $\zeta$ and $\delta$ are the vertical component of relative vorticity and the horizontal divergence, respectively. The vertical velocity in the Fourier space can then be obtained by using Eqs. (57) and (58).

Again, we assume a bell-shaped warm region associated with low-level sensible heating:

$$T'(x,y) = \frac{T'_o}{(r^2/b^2+1)^{3/2}}. \tag{59}$$

To a first approximation, the diabatic heating rate associated with the above specified warm region in a basic flow ($U$) can be specified as

$$\frac{q'}{c_p} = \frac{D\theta}{Dt} = U\frac{\partial T'}{\partial x} + \left(\frac{N^2\theta_o}{g}\right)w'. \tag{60}$$

As discussed in Malkus and Stern (1953), the diabatic heating rate is mainly created and maintained by horizontal temperature advection due to small-scale turbulence and is not altered significantly by convective motions of the scale of $w'$. Thus, the last term of the above equation may be neglected. After carrying out the Fourier transform of Eq. (59) and the approximated form of Eq. (60), we have

$$\hat{h}(k,l) = iT_o k e^{-K}/2\pi. \tag{61}$$

Substituting Eq. (61) into Eqs. (57) and (58) in Fourier space, the variables $\hat{p}$, $\hat{w}$, $\hat{u}$, $\hat{v}$, $\hat{\zeta}$, and $\hat{\delta}$ can be solved analytically in the Fourier space and then transformed back to the physical space numerically using a Fast Fourier transform (FFT) algorithm.

Figure 16 shows a case of quasi-geostrophic inviscid flow over an isolated warm region which has a maximum temperature and a half-width of 7.5 and 1, respectively. The basic flow blows from left to right. According to Eq. (60), there exists heating (cooling) upstream (downstream) of the center of the warm region. Both $R_o$ and $\gamma$ have a value of 0.2. The dimensional parameters may be considered as $U$=10 m s$^{-1}$, $b$=500 km, $f$=10$^{-4}$ s$^{-1}$, $N$=0.01 s$^{-1}$, $H_1$=1 km, $H_o$=5 km, and $T_o$=20 K. The response of the atmosphere to the heating and cooling associated with the warm region at $z$=0.05 (250 m) is an upward (downward) motion upstream (downstream) of the center of the warm region (Fig. 16a). Upstream (downstream) of the region of upward (downward) motion, there exists a region of weak compensating downward (upward) motion. In fact, the vertical velocity field is in phase with the diabatic heating. The thermal forcing produces a region of high buoyancy (less dense) air in the vicinity of the warm region (Fig. 16b). The buoyancy is defined as $g\theta'/\theta_o$, which then produces the low pressure region near the surface (Fig. 16c) as required by the hydrostatic balance. On both the upstream and downstream sides of the region of high buoyancy and low pressure, there exist regions of weak low buoyancy and high pressure, respectively. At this level ($z$=0.05), the air parcel experiences a cyclonic circulation near the center of the low pressure region, where there exists a cell of positive relative vorticity (Figs. 16d and e). Two regions of weak negative vorticity appear to be on both

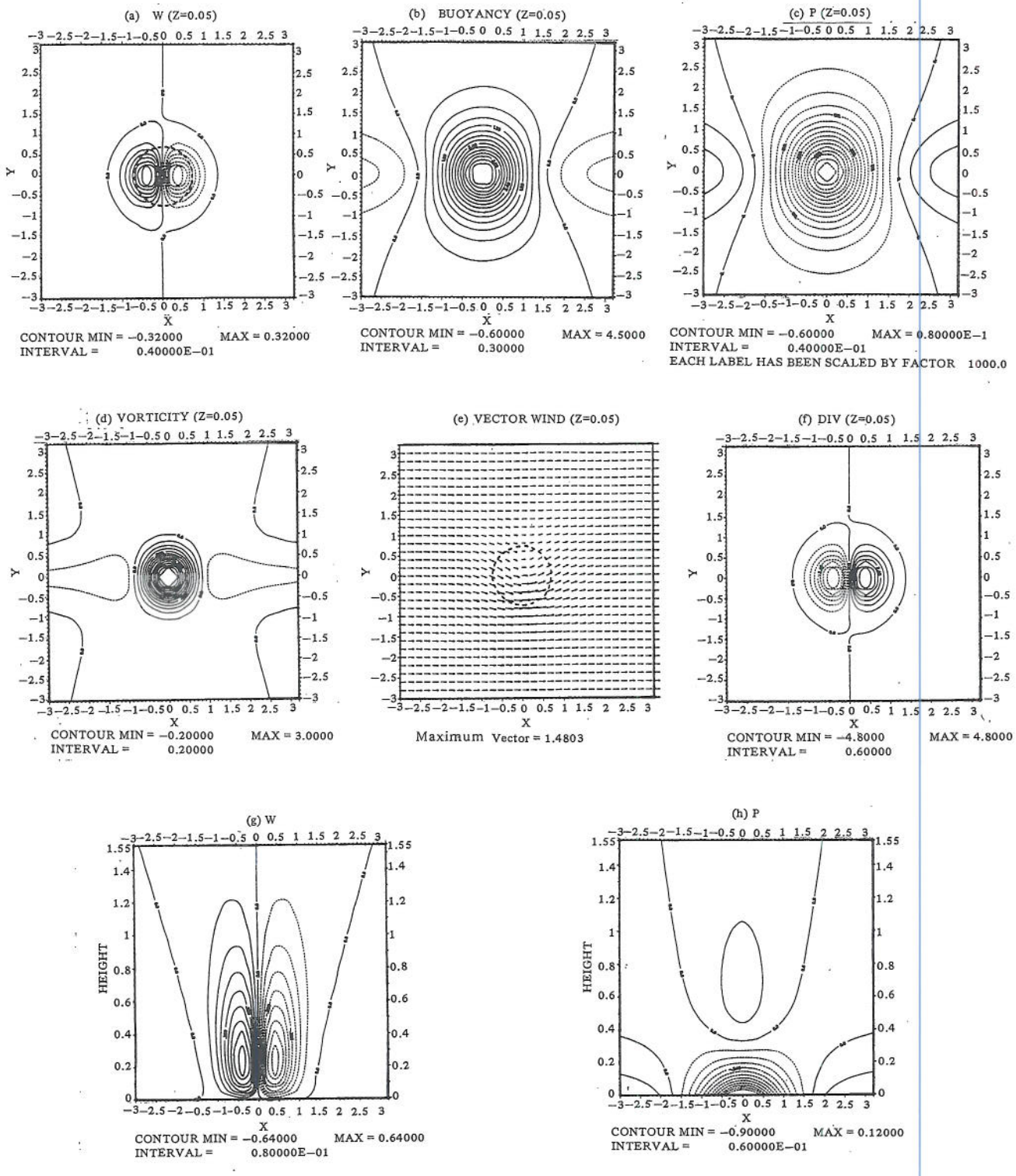


**Fig. 16.** Inviscid quasi-geostrophic barotropic flow over a bell-shaped warm region with a maximum perturbation potential temperature ($T_o$) and the half-width (b) of 7.5 and 1, respectively. The parameters associated with the basic flow are: $R_o$=0.2, $\gamma$=0.2, $E$=0. Six horizontal fields at $z$=0.05 are shown: (a) vertical velocity, (b) buoyancy, (c) perturbation pressure, (d) relative vorticity, (e) horizontal vector wind, and (f) divergence. Two cross sections along $y$=0 are shown: (g) vertical velocity and (h) perturbation pressure. The thick dashed lines in (a) and (e) indicate the contour of $T$=4. Notice that all variables are nondimensionalized. (From Lin, 1989a)

the upstream and downstream sides of the positive vorticity. Notice that the relative vorticity reaches a maximum of about 0.6*f*, which is relatively high for the quasi-geostrophic approximation to be valid. Figure 16f shows the divergence field at $z$=0.05, which has a convergence (divergence) upstream (downstream) of the center of the warm region. The divergence field is related to the vertical motion by the relationship $\delta=-w_z$.

Figures 16g and h display the vertical cross sections of the vertical velocity and perturbation pressure along $y$=0. The vertical velocity field (Fig. 16g) near the warm region center is mainly dominated by an upward motion upstream followed by a downward motion. The absolute value of the vertical velocity increases with height until $z$=0.2 and then decreases. Weak compensative downward and upward motions are found far upstream and downstream, respectively. The air parcel is lifted near the center of the warm region and displaced slightly downward far upstream and downstream. There exists a strong vortex stretching near the center of the warm region and two regions of weak vortex compression far upstream and downstream. The pressure perturbation (Fig. 16h) is almost confined below the e-folding depth of the heating, i.e., $z$=0.2. Near the warm region center, the perturbation pressure decreases exponentially with height and reverses its phase at a level of about $z$=0.35. The resulting high pressure is associated with the compensative divergence at this level, instead of convergence at the lower level. The amplitude of the perturbation pressure decays exponentially with height as also can be detected from the solution, Eq. (57).

To investigate the inertial effects, we may combine Eqs. (43)-(47) into a single equation for $w$:

$$R_o^2 w_{xxzz} + w_{zz} + \nabla_H^2 w = \nabla_H^2 q . \tag{62}$$

Making Fourier transforms of the above equation and Eq. (53) gives

$$\hat{w}_{zz} + \frac{K^2}{R_o^2 k^2 - 1}\hat{w} = \frac{\hat{h} K^2 e^{-z/\gamma}}{R_o^2 k^2 - 1} . \tag{63}$$

The general solution of the above equation can be written as

$$\hat{w} = A \exp( iKz/\sqrt{(R_o^2 k^2 - 1)} ) + B \exp( -iKz/\sqrt{(R_o^2 k^2 - 1)} ) + \frac{\hat{h}\gamma^2 K^2 e^{-z/\gamma}}{\gamma^2 K^2 + (R_o^2 k^2 - 1)} . \tag{64}$$

The lower boundary condition requires $w$=0 at $z$=0. The solution is composed of two parts: (a) $R_o^2 k^2 > 1$ and (b) $R_o^2 k^2 < 1$. For $R_o^2 k^2 > 1$, the upper boundary condition requires $B$=0 to allow the energy to radiate upward to infinity. Thus, the solution in this upward propagating wave regime can be obtained:

$$\hat{w} = \frac{-\hat{h}\gamma^2 K^2}{\gamma^2 K^2 + (R_o^2 k^2 - 1)} [ e^{iKz/(R_o^2 k^2 - 1)^{1/2}} - e^{-z/\gamma} ], \quad \text{for } R_o^2 k^2 > 1 . \tag{65}$$

The solution in the other regime ($R_o^2 k^2 < 1$) can be obtained in a similar way except it requires the solution to vanish at infinity. As discussed in Part I (Lin, 1994), this regime is called the evanescent wave regime. The solution reads

$$\hat{w} = \frac{-\hat{h}\gamma^2 K^2}{\gamma^2 K^2 - (1 - R_o^2 k^2)} [ e^{-Kz/(1 - R_o^2 k^2)^{1/2}} - e^{-z/\gamma} ] \quad \text{for } R_o^2 k^2 > 1 . \tag{66}$$

The other variables can be obtained:

$$\hat{p} = \frac{1}{ik} [ \int_z^\infty \hat{w}\, dz - \int_z^\infty \hat{h} e^{-z/\gamma} dz ], \tag{67}$$

$$\hat{u} = \frac{R_o^2 k^2 - il}{1 - R_o^2 k^2}\hat{p} , \tag{68}$$

$$\hat{v} = \frac{R_o^2 kl + ik}{1 - R_o^2 k^2}\hat{p} , \tag{69}$$

$$\hat{b} = \frac{1}{ik}(\hat{q} - \hat{w}) , \tag{70}$$

$$\hat{\zeta} = -K^2 \hat{p} - i R_o^2 k \hat{w}_z , \tag{71}$$

$$\hat{\delta} = -R_o \hat{w}_z . \tag{72}$$

Figure 17 shows an example of an inviscid flow with $R_o$=1 past an isolated warm region. The parameters associated with the flow and the diabatic source/sink are $\gamma$=1 and $T_o$=1.5. The dimensional parameters may be considered as $U$=10 ms$^{-1}$, $b$=100 km, $f$=10$^{-4}$ s$^{-1}$, $N$=0.01 s$^{-1}$, $H_1$=1 km, $H_o$=1 km, and $T_o'$ =4 K. The response of the fluid to the diabatic heating at $z$=0.25, corresponding to a dimensional height of 250 m, is an upward motion upstream and near the center of the warm region followed by a downward motion downstream (Fig. 17a). Compared with the quasi-geo-

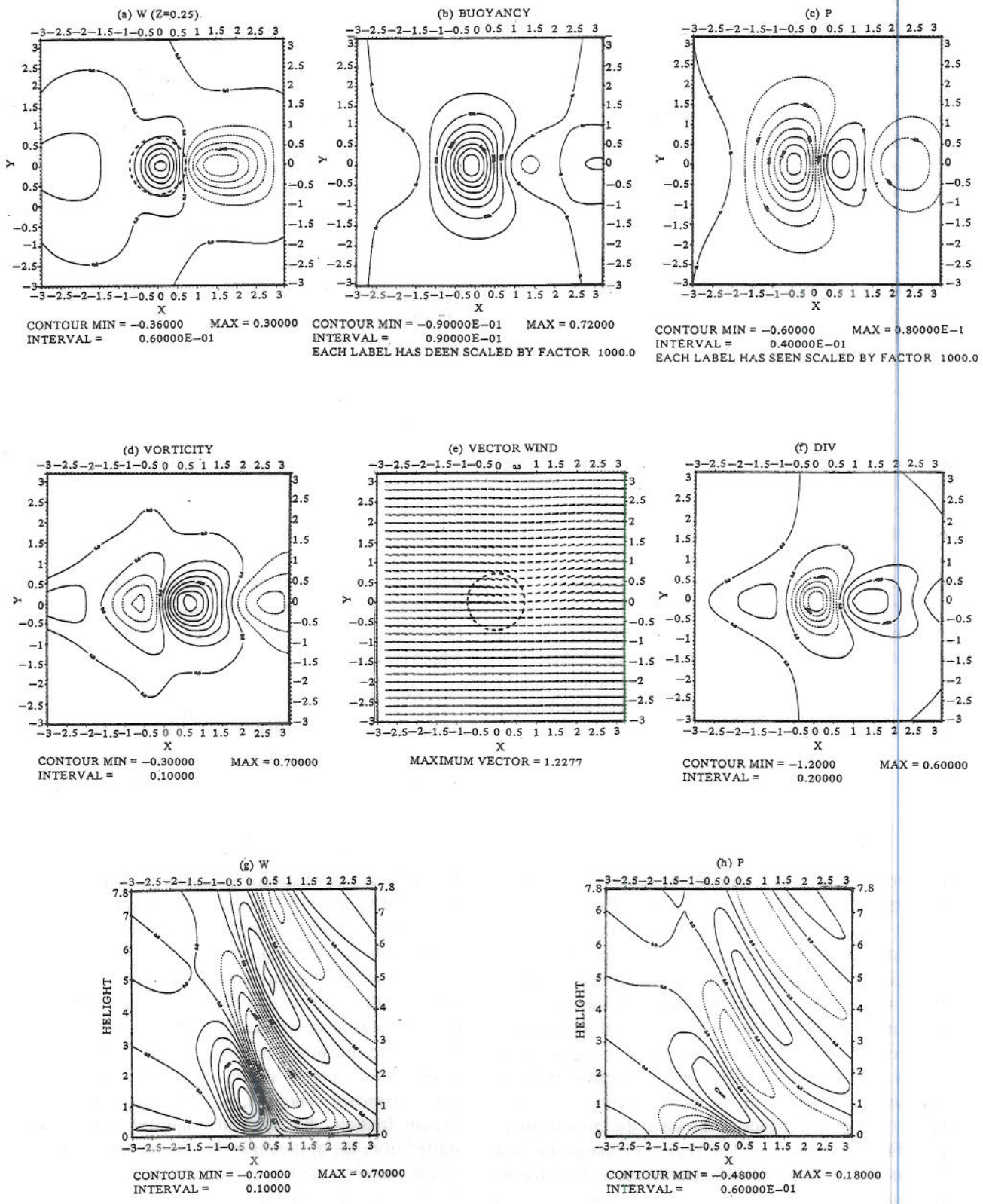


**Fig. 17.** Same as Fig. 16 except with inertial effects included. The parameters used are: $T_o$=1.5, $b$=1, $R_o$=1, and $\gamma$=1. Solutions can be found in Eqs. (65)-(72). (From Lin, 1989a)

strophic case (Fig. 16), the major regions of upward and downward motion are shifted downstream. This can be explained by the advection effect because the inertial terms, i.e., the $R_o$ terms, play a significant role in the present case. Even though not shown in Fig. 17a, there still exists a weak compensative downward motion associated with the major region of upward motion (Fig. 17g). The horizontal pattern of the vertical velocity is more asymmetric in the basic wind direction than that in the quasi-geostrophic case. The buoyancy field (Fig. 17b) is similar to that of the quasi-geostrophic case, except there exists a region of high buoyancy (less dense) air far downstream. The major region of high buoyancy near the center of the warm region is mainly produced by the diabatic heatingand cooling. The indirect effect on the buoyancy due to vertical motion (Eq. (48)) is not pronounced at such a low level because the vertical velocity is weak near the surface.

The perturbation pressure pattern (Fig. 17c) is no longer as similar to the perturbation buoyancy pattern as that of the quasi-geostrophic case. This is mainly caused by the vertical propagation of the thermally induced inertia-gravity waves. In fact, the pressure field is almost out of phase with the buoyancy field. The V-shaped (or U-shaped as used by Smith, 1980) pattern of the perturbation pressure, also pronounced in other fields, is an indication of the upward propagation of energy as shown in a nonrotating mountain wave problem (Smith, 1980) and in a nonrotating diabatic heating problem (Lin, 1986a; Lin and Li, 1988). The group velocity calculation of Smith can be extended to include the Coriolis force, which gives the concentrated region of the wave energy:

$$y^2=[\frac{z\,l^2(R_o^2k^2-1)^{1/2}}{k(R_o^2l^2-1)(k^2+l^2)^{1/2}}]x,\quad \text{for } R_o^2k^2>1 \qquad (73)$$

With no rotation, the above equation reduces to the formula derived by Smith. With the rotational effect included, the wave energy is still concentrated near the parabola des-cribed by the above equation. However, the latus rectum becomes larger compared to the nonrotating case. In addition, the above equation indicates that only the wave part of the disturbance contributes to the upward propagation of the energy. Therefore, the V-shape is less pronounced for a flow with a smaller Rossby number. Further evidence for upward propagation of the wave energy is the upstream tilt of the disturbance as shown in the cross sections at $y$=0 (Figs. 17g and h). The region of maximum and minimum perturbations are shifted farther downstream with height, which indicates that the wave energy is both propagated upward and advected downstream. The vorticity field indicates that there exists a negative vorticity center just upstream of the warm region center, followed by a strong positive vorticity center and a negative vorticity center far downstream (Fig. 17d). The significant difference from the quasi-geostrophic case is that the positive (negative) vorticity is associated with the high (low) pressure and not the low (high) pressure. The positive vorticity is no longer in phase with the low because the vertical velocity term is as important as the pressure term in Eq. (71) for a flow with a larger Rossby number. This distinction has also been made in a study of a low-Froude number flow over mesoscale mountains, such as the Central Mountain Range of Taiwan, by Lin *et al.* (1992). In their case, the Taiwan mesolow does not coincide with the mesovortex. The mesolow is located on the southeast slope of the mountain, while the mesovortices are drifting downstream with the basic wind.

Due to the weaker rotational effect, the vector wind does not deflect as strongly as for the quasi-geostrophic case. However, the cyclonic flow around the region of positive vorticity, not the low pressure, is still evident in this case (Fig. 17e). The divergence field is related to the vertical velocity field by Eq. (72) (Fig. 17f). A region of convergence near the center of the warm region is accompanied by two regions of divergence upstream and downstream. Figures 17g and h show the cross sections of the vertical velocity and perturbation pressure along $y$=0. The major difference from the quasi-geostrophic case is that the phase tilts upstream with height. The perturbation pressure field is in phase with the vertical velocity overall, which indicates that the wave energy is propagated upward because the vertical energy flux, $\int p'w'\,dx$, is positive (Eliassen and Palm, 1960; Jones, 1967).

With the Ekman friction included in the quasi-geostrophic flow, there are three significant features of the resulting disturbance: (1) an upstream-downstream asymmetry, (2) an upstream phase tilt in the lower layer, and (3) weakening of the positive vorticity and the low (Lin, 1989a). The upstream-downstream asymmetry is similar to that of Buzzi and Tibaldi (1977) for a quasi-geostrophic flow over a mountain. The low-level upstream phase tilt is consistent with that of Smagorinsky (1953), who investigated the response of a quasi-geostrophic flow over a diabatic source with $\beta$ effects and baroclinicity included. These two phenomena are explained by the following argument. At $z$=0, the maximum positive vorticity is located at the warm region center as shown in Fig. 16. According to the lower boundary condition, Eq. (50), associated with the Ekman friction, the maximum upward motion will be shifted from the upstream in the interior fluid to the warm region center at the top of the Ekman layer ($z$=0). Thus, there exists an upstream phase tilt with height in the lower layer. The disturbance associated with the upward motion is then advected by the basic wind, which gives the asymmetric pattern of the vertical velocity.

## 2. Baroclinic Flow

The development of this theory of coastal cyclogenesis is analogous to the development of the theory of lee cyclogenesis proposed by Smith (1984, 1986). Both quasi-geostrophic and semigeostrophic flow over a low-level diabatic heat source have been investigated by Lin (1989b, 1990a) and will be reviewed below.

For an inviscid Boussinesq fluid on an f-plane with constant basic state stratification, the linearized quasi-geostrophic potential vorticity equation and the thermodynamic equation applied at the surface can be written as (e.g., see Smith, 1984; Bannon, 1986)

$$\left(\frac{\partial}{\partial t}+U\frac{\partial}{\partial x}+V\frac{\partial}{\partial y}\right)\left(\nabla_H^2 p'+\frac{f^2}{N^2}p'_{zz}\right)$$

$$=\left(\frac{g\rho_o f^2}{c_p T_o N^2}\right)q'_z \qquad (74)$$

$$\left(\frac{\partial}{\partial t}+U\frac{\partial}{\partial x}+V\frac{\partial}{\partial y}\right)\theta'+u'_g\Theta_x+v'_g\Theta_y+w'\Theta_z$$

$$=\left(\frac{\theta_o}{c_p T_o}\right)q', \qquad (75)$$

where subscripts denote partial differentiation. With the hydrostatic, geostrophic wind and thermal wind equations,

$$\theta'=(\theta_o/g\rho_o)p'_z, \qquad (76)$$

$$u'_g=(-1/f\rho_o)p'_y;\ v'_g=(1/f\rho_o)p'_x, \qquad (77)$$

$$U_z=(-g/f\theta_o)\Theta_y;\ V_z=(g/f\theta_o)\Theta_x, \qquad (78)$$

Eq. (75) becomes

$$\left(\frac{\partial}{\partial t}+U\frac{\partial}{\partial x}+V\frac{\partial}{\partial y}\right)p'_z-(U_z p'_x+V_z p'_y)+\rho_o N^2 w'$$

$$=\left(\frac{g\rho_o}{c_p T_o}\right)q' \qquad \text{at } z=0. \qquad (79)$$

The baroclinic waves associated with the system of Eqs. (74) and (79) are dispersive waves with real frequencies (Smith, 1984), which can propagate along the surface of the earth in the presence of a horizontal temperature gradient.

The deformation depth or Rossby depth of the flow, $H_o=fL/N$, has a value of about 10 km for a flow with $f=10^{-4}$ s$^{-1}$, $L$ (horizontal scale) = 1000 km, and $N=10^{-2}$ s$^{-1}$. Compared with the deformation depth, the thickness of the diabatic heating (~1km) is very small. In this way, we may assume that there exists no interior thermal forcing as a first approximation. Using the shallow heating assumption, Eq. (74) reduces to the homogeneous form:

$$\nabla_H^2 p'+\left(\frac{f}{N}\right)^2 p'_{zz}=0. \qquad (80)$$

In deriving the above equation, we have assumed that there exists no initial potential vorticity anomaly. Making the Fourier transform of the above equation and applying the upper boundary condition, which requires the solution to be bounded at infinity, and the lower boundary condition, which requires $w=0$ at $z=0$ for a flow over a flat surface, we obtain

$$\hat{p}_t+\left[ik\left(U_o+\frac{fU_z}{N|K|}\right)+il\left(V_o+\frac{fV_z}{N|K|}\right)\right]\hat{p}$$

$$=\left(\frac{-g\rho_o f}{c_p T_o N|K|}\right)\hat{q}, \qquad (81)$$

where $U_o$ and $V_o$ are the surface wind speeds in the $x$ and $y$ directions, respectively. The vertical shears, $U_z$ and $V_z$, are assumed to be constant.

The above equation is similar to Eq. (4.1) of Smith (1984) except for the forcing term. Similar to the uniform flow case, the heating rate may be approximated by

$$q'(x,y)=c_p\left(U_o\frac{\partial}{\partial x}+V_o\frac{\partial}{\partial y}\right)T'(x,y). \qquad (82)$$

Making the Fourier transform of the above equation and by straightforward manipulation of Eq. (4.1) of Smith (1984) and Eq. (81), we obtain a relationship between the orographic forcing and the thermal forcing, namely,

$$h_m(x,y)=\left(\frac{-g}{T_o N^2}\right)T'(x,y), \qquad (83)$$

where $h_m(x, y)$ is the shape of the mountain. The above equation means that the response of a quasi-geostrophic flow over a stationary cold (warm) region is equivalent to that over a mountain (valley) if the forcings are of the same shape. According to the above equation, a cold region with a potential temperature anomaly of 5.3 K corresponds to a mountain with a height of 2 km if $T_o=260$ K and $N=0.01$ s$^{-1}$. This analogy has also been illustrated by Smith (1979), where an anticyclonic circulation can be produced by a quasi-geostrophic flow over either a mountain or a cold dome.

The solution of Eq. (81) can be found by assuming that there exists no pressure perturbation initially:

$$\hat{p}(k,l,z,t)=\left(\frac{-g\rho_o f}{c_p T_o N|K|}\right)$$

$$\cdot\frac{\hat{q}(k,l)(1-e^{-Bt})e^{-N|K|z/f}}{B}, \qquad (84)$$

where

$$B\equiv ik\left(U_o+\frac{fU_z}{N|K|}\right)+il\left(V_o+\frac{fV_z}{N|K|}\right). \qquad (85)$$

The perturbation pressure in the physical domain is then recovered by the inverse Fourier transform. Equation (84) describes the formation of a baroclinic cyclone if there exists a level at which the basic wind reverses direction, as will be discussed later. This is similar to the lee cyclogenesis problem as studied in Smith (1984, 1986). We thus propose this mechanism as a possible prototype of East Coast cyclogenesis. The problem is also similar to the Eady model (Eady, 1949) except that the rigid lid assumption is removed. In this way, the baroclinic instability of the Eady type is avoided (e.g., Pedlosky, 1982).

*A. Quasi-Geostrophic Baroclinic Wave Generation by Two-Dimensional Diabatic Heating*

For a two-dimensional quasi-geostrophic flow with diabatic heating, Eq. (84) reduces to

$$p'(x,z,t)=\left(\frac{-g\rho_o f}{c_p T_o N}\right)\int_{-\infty}^{\infty}\frac{\hat{q}(k)(1-e^{-Bt})e^{-N|k|z/f}}{|k|B}$$

$$\cdot e^{ikx}dk, \qquad (86)$$

where

$$B=ik(U_o+H_o U_z);\ H_o=f/N|k|. \qquad (87)$$

As discussed by Smith (1984), the integral in Eq. (86) will go to zero ($p\to 0$) as $|x|\to\infty$ due to the rapid oscillation of the exp($ikx$) term if the integrand is well behaved according to the Riemann-Lebesque lemma (Lighthill, 1970). This implies that the disturbance will remain locally in the vicinity of the diabatic heat source/sink. The baroclinic waves can only be generated if the denominator of the integrand vanishes for some value of $k$. This is possible if $U_o$ and $U_z$ have opposite signs, i.e., if there exists a back-sheared basic flow and a wind reversal level ($|k^*|=f/NH^*=-fU_z/NU_o$). An asymptotic solution for large $x$ and $t$, similar to that of Smith (1986), can be obtained, which describes a train of baroclinic waves extending from the center of the diabatic heating to the moving point $x=U_o t$. A bell-shaped heat source/sink in the $x$ direction with a horizontal scale of $b$, such as that of Eq. (93) of Lin (1994), can be used. A Fast Fourier Transform (FFT) algorithm is then employed to obtain the solution in physical space.

Figure 18 shows an example of a baroclinic quasi-geostrophic flow over a diabatic cooling with a cooling rate of -0.24 J(kg-s)$^{-1}$ and a half-width of 75 km. The basic wind is assumed to be of the form $U(z)=(-10+0.005z)$ ms$^{-1}$. This gives a wind reversal level of 2 km. The grid interval and the number of grid points in the $x$ direction used in the calculation are 30 km and 128, respectively. After 6 hr (Fig. 18a), there exists a region of perturbation high pressure near the center of diabatic cooling ($x$=0). The high is associated hydrostatically with cold air near the cooling center. On the downstream side ($x$<0), there exists a wider region of weak low-pressure perturbation. The disturbance decays exponentially with height as indicated by Eq. (86). After 12 hr (Fig. 18b), the perturbation high pressure strengthens to a value of about 3.4 mb, while the perturbation low pressure deepens gently to a value of about -1.5 mb. After 18 hr (Fig. 18c), the high pressure deepens to about 3.6 mb, while the low pressure increases to about -3.8 mb. After 24 hr (Fig. 18d), the high pressure weakens to about 3.2 mb, while the low pressure keeps strengthening to a value of -5.6 mb. The upshear vertical tilt of the trough is evidence of the baroclinic wave generated by the diabatic heating. This allows the heat flux to be transported northward meridionally (in the positive $y$ direction) (e.g., see Gill, 1982). The phase line of the trough becomes more vertical at the later stage (not shown). Once the available potential energy (APE) stored in the basic baroclinic current has been transferred to the forced baroclinic waves, the phase line will become vertical. For the present case with $H$=2 km (wind reversal level), the theory predicts a reasonable wavelength of 1250 km ($\lambda=2\pi/k^*=2\pi NH/f$) of the baroclinic wave with a dipolar structure.

Figure 19 shows the time evolution of the absolute minimum and maximum surface perturbation pressures for the case of Fig. 18. The perturbation high pressure grows rather rapidly in the early stage, reaches its maximum of 3.65 mb at 17 hr, and then decays gradually afterwards. The perturbation low pressure develops rather slowly in the first 12 hr, and then deepens much more rapidly at the later stage. The rapid development of the perturbation low pressure after 12 hr can be explained by a group velocity argument. The group velocity of the baroclinic wave (Smith, 1984, 1986) is

$$c_g=U(H)-\frac{f}{N|k|^3}(k\cdot U_z)k, \qquad (88)$$

where $H=f/N|k|$ and $U(z)=U_o+U_z z$. The above

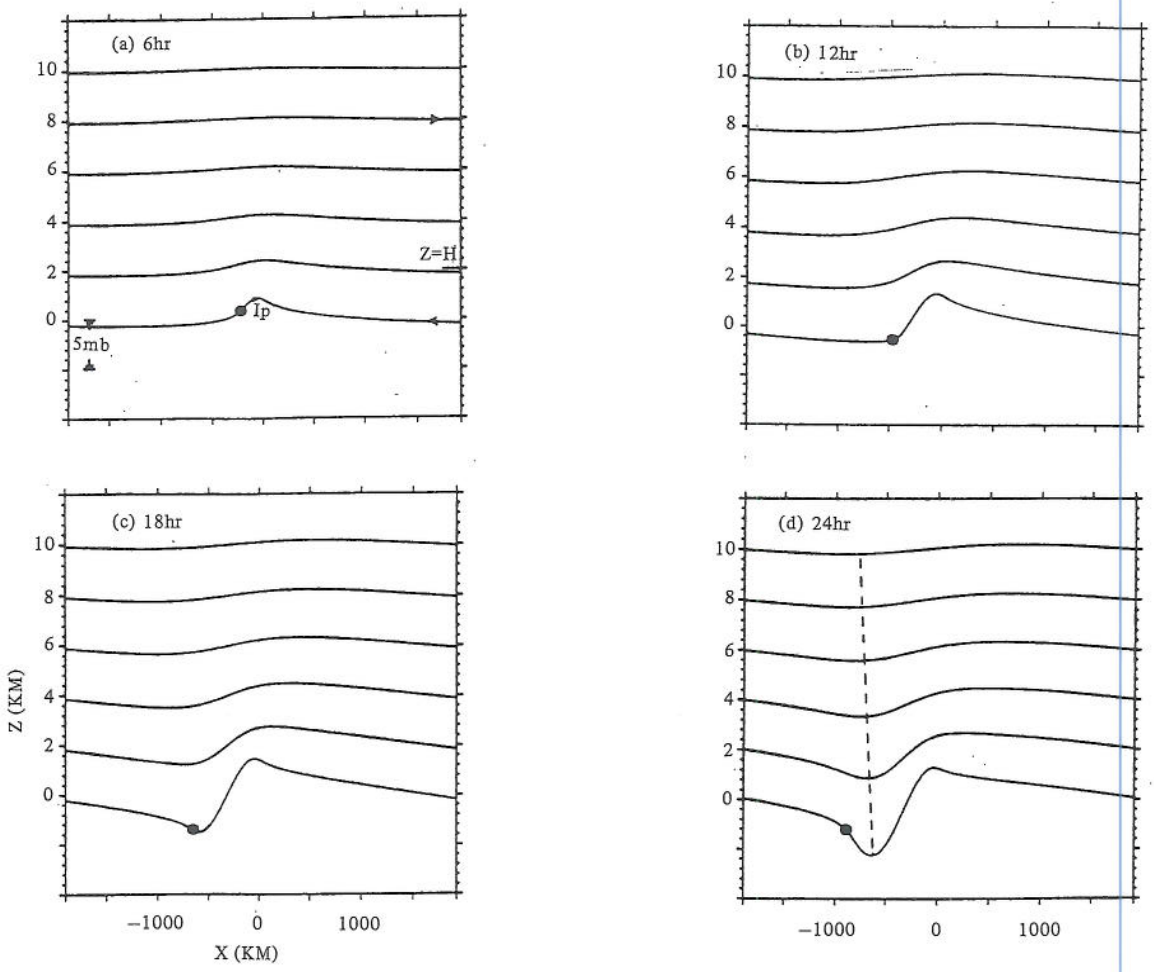


**Fig. 18.** Two-dimensional baroclinic waves forced by diabatic cooling with a cooling rate of -0.24 J (kg-s)$^{-1}$ and half-width of 75 km. The solution is given by Eq. (81) with $U(z)=(-10+0.005z)$ ms$^{-1}$. Other parameters are: $f=10^{-4}$ s$^{-1}$, $N=10^{-2}$ s$^{-1}$, $T_o=260$ K, and $\rho_o=1$ kg m$^{-3}$. Six levels and four time steps of perturbation pressures are shown: (a) 6 h, (b) 12 h, (c) 18 h, and (d) 24 h. The wind reversal level is located at 2 km (labeled by $z=H$). The location of an air parcel, originating at $x=0$ and moving with the group velocity ($c_g=U_o=-10$ ms$^{-1}$), is indicated by a dot at each time step. The arrows in (a) illustrate the direction of the basic wind. The dashed line in (d) is a constant phase line. (From Lin, 1989b)

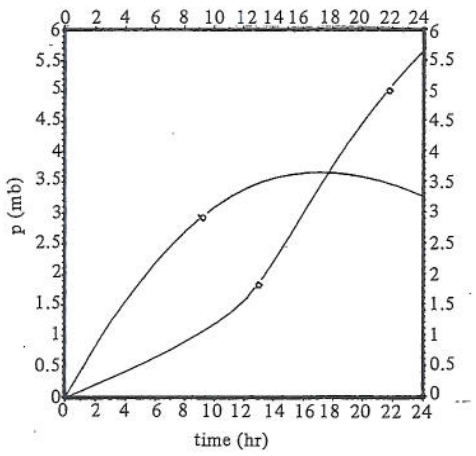


**Fig. 19.** Time evolution of absolute minimum (a) and maximum (b) surface perturbation pressures for the case of Fig. 18.

equation reduces to $c_{gz}=U_o$ for a two-dimensional wave (Smith, 1984). As indicated in Eq. (82), a moving airstream over the diabatic cooling, $q'(x)=Q_o/[1+(x/b)^2]$, corresponds to that over a cold region extending from $x=0$ to $-\infty$, $T'(x)=(Q_o b/c_p U_o)\tan^{-1}(x/b)$. This is analogous to an airflow over a flat plain from a plateau, according to Eq. (83). Therefore, the fluid is trying to form a high in the vicinity of the cooling center ($x=0$) and a first trough downstream ($x<0$). For example, consider an air parcel originating at $x=0$ near the surface (denoted by a dot in Fig. 18). It will take 12 hr to advect to 432 km (i.e., $x=-432$ km in the figure) downstream at the group velocity $c_g=U_o=-10$ ms$^{-1}$, which is approximately the region of the developing low (Fig. 18b). During the 12 to 24 hr period, the air parcel reaches the region of the developing low. Thus, the low deepens much more rapidly at this stage (Figs. 18c and 19). Like the perturbation high pressure near the cooling center, the perturbation low pressure will reach a

minimum and increase its amplitude afterwards since the air parcel originating at $x$=0 near the surface will pass through the region of the well-developed low. Thus we may conclude that the diabatic heating plays an important role in converting the available potential energy stored in the baroclinic current to the thermally forced baroclinic wave.

To show the importance of the baroclinicity and the existence of the wind-reversal level in the above cyclogenesis mechanism, we perform four cases similar to the one outlined above, except that now the baroclinicity and wind-reversal level do not exist (Fig. 20). For quasi-geostrophic, baroclinic flow over the diabatic heat source with forward shear (i.e., no wind reversal, Figs. 20a and b), the disturbance is much weaker compared with the corresponding cases with wind reversal (Fig. 18). This indicates that forward vertical wind shear tends to suppress the development of the low or high pressure. For quasi-geostrophic, barotropic flow over the diabatic heating (cooling) region, a perturbation low (high) of -5 mb (+5 mb) is produced after 24 hr (Figs. 20c and d). The surface low (high) produced by the diabatic heating (cooling) is located about 400 km downstream of the heating (cooling) center. Notice that a moving airstream over the diabatic heating corresponds to that over a warm region extending from $x$=0 to -∞, but with the gradient concentrated in the region of the diabatic heating, for Fig. 20c. The low pressure at the surface is produced by the less dense air above the warm region in a barotropic flow as required by the hydrostatic equation. Thus the low pressure forms on the warm side or the downstream side of the diabatic heating center ($x$=0). The results are consistent with the quasi-geostrophic flow over a warm region as discussed earlier in Section III.1. The response is quite different from the low-high couplet produced by diabatic heating in a backsheared baroclinic flow.

### *B. Three-Dimensional Response*

Some interesting discussions (Bannon, 1990; Lin, 1990b) have been presented since the publication of the above proposed cyclogenesis mechanism by Lin (1989b). The major comments of Bannon on Lin's work are: (a) the forcing scale is too small to use the quasi-geostrophic approximation, and (b) the vertical distribution of the surface

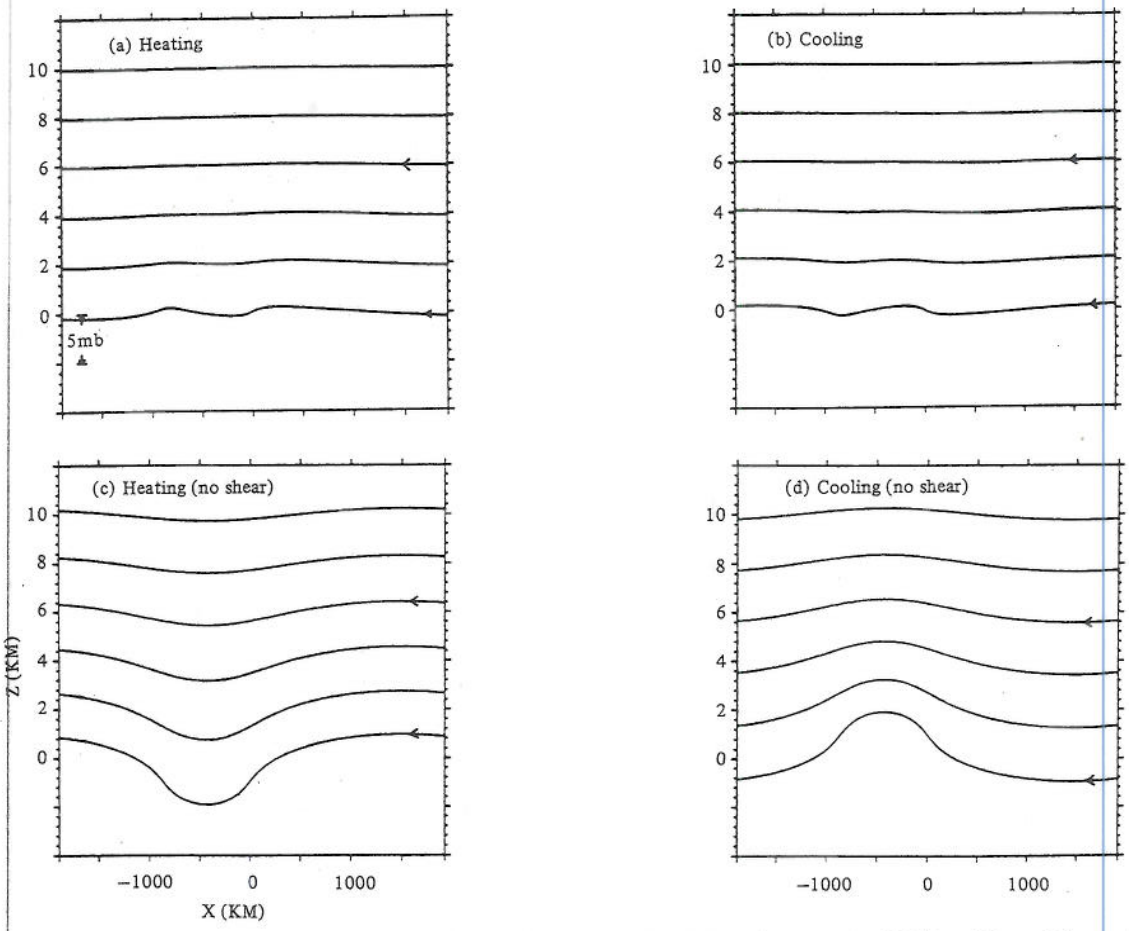


**Fig. 20.** Six levels of perturbation pressures after 24 h are shown for four cases: (a) $Q_o$=0.24 J (kg–s)$^{-1}$, $U(z)$=(-10 – 0.005$z$) ms$^{-1}$ (forward shear with heating), (b) same as (a) except with $Q_o$=-0.24 J (kg–s)$^{-1}$ (forward shear with cooling), (c) $Q_o$=0.24 J (kg–s)$^{-1}$ (no shear with heating), and (d) same as (c) except with $Q_o$=-0.24 J (kg–s)$^{-1}$ (no shear with cooling). The heating function is the same as that prescribed in Fig. 18.

heating should be included. It was discussed in Lin's reply (1990b) that the heating scale should be considered to be larger than its half-width and that the cyclone scale is not directly proportional to the forcing scale in a transient flow, unlike the steady state flow over a mountain. In addition, the quasi-geostrophic approximation was improved in a subsequent paper (Lin, 1990a) using the geostrophic momentum approximation in a semigeostrophic model. In the second comment (b), it was shown by Lin (1990b) that the contribution of the vertical distribution of the surface heating does not alter the low to be a high as claimed by Bannon (1990). In the following, we will show some recent results of a continuously stratified baroclinic flow over a vertically distributed heat source.

Using the geostrophic momentum approximation (Eliassen, 1962; Hoskins, 1975), the nonlinear ageostrophic advection of the geostrophic wind can be included in the model. The governing equations in the geostrophic space may be written as

$$[\frac{\partial}{\partial T}+(U-\frac{1}{\rho_o f}\Pi'_Y)\frac{\partial}{\partial X}+(V+\frac{1}{\rho_o f}\Pi'_X)\frac{\partial}{\partial Y}]Q_g$$

$$=(\frac{g\rho_o f^2}{c_p T_o N^2})q'_Z \tag{89}$$

$$\Pi'_{ZT}+(U_o-\frac{1}{\rho_o f}\Pi'_Y)\Pi'_{ZX}+(V_o+\frac{1}{\rho_o f}\Pi'_X)\Pi'_{ZY}$$

$$-U_Z\Pi'_X-V_Z\Pi'_Y+\rho_o N^2 w'=(\frac{g\rho_o}{c_p T_o})q'$$

$$\text{at } Z=0, Z_T, \tag{90}$$

where

$$Q_g=\nabla_H^2\Pi'+\frac{f^2}{N^2}\Pi'_{ZZ}, \tag{91a}$$

$$X=x+\frac{v_g}{f}, \tag{91b}$$

$$Y=y-\frac{u_g}{f}, \tag{91c}$$

$$Z=z, \tag{91d}$$

$$T=t, \tag{91e}$$

$$\Pi=p+\frac{\rho_o}{2}(u_g^2+v_g^2). \tag{91f}$$

The potential vorticity is then equal to $Q_g/\rho_o f$. Similar to that in Lin (1990a), the pressure in the geostrophic space is separated into a basic part and a disturbance part, i.e., $\Pi(T, X, Y, Z)=\Pi(Z)+\Pi'(T, X, Y, Z)$. The basic part is assumed to satisfy the hydrostatic balance,

$$\frac{1}{\rho_o}\frac{\partial\Pi}{\partial Z}=\frac{g\Theta}{\theta_o}. \tag{92}$$

The lower boundary condition with the mountain and Ekman friction included may be written as

$$w'(T,X,Y)=[\frac{\partial}{\partial T}+(U_o+u_g)\frac{\partial}{\partial X}+(V_o+v_g)\frac{\partial}{\partial Y}]$$

$$\cdot h_m(T,X,Y)+\frac{\sqrt{\nu/2f}}{\rho_o f}\nabla_H^2\Pi'(T,X,Y)$$

$$\text{at } Z=0,$$

and the upper boundary condition at the imposed rigid lid is

$$w'(T, X, Y)=0 \qquad \text{at } Z=Z_T. \tag{93}$$

In the above equation, we have implemented a simple Ekman layer boundary condition as described earlier in Section III.1. The Ekman number corresponds to $\nu/fH_o^2$, where $H_o$ is a height scale. We then substitute Eq. (93) into Eq. (90) for the lower boundary condition. The system of Eqs. (89) and (90) can be solved numerically by the leap-frog and the second-order center-difference schemes applied to the time and space derivatives, respectively. The pressure perturbation in the geostrophic space $\Pi'$ can be solved from Eq.(91a) in the Fourier space and transformed back to the geostrophic space numerically by an FFT algorithm. The variables in the physical space are then recovered by applying the inverse geostrophic transformation based on Eqs. (91b)-(91f). In the following, we have used the following numerical parameters: $\Delta t$=10 min, $\Delta x=\Delta y$=60 km. The total grid numbers are 64 in both the $x$ and $y$ directions. As mentioned earlier, a bounded upper boundary condition is applied at $z$=10 km. A periodic lateral boundary condition is assumed implicitly by the use of an FFT algorithm.

To check the model, we perform a simulation of baroclinic flow over a bell-shaped mountain. The mountain shape is assumed to be

$$h_m(x,y)=\frac{h_o}{[x^2/a_x^2+y^2/a_y^2+1]^{3/2}}, \tag{94}$$

where $a_x$ and $a_y$ are the horizontal scales of the mountain in the $x$ and $y$ directions, respectively. The mountain

height ($h_o$) and the horizontal scale ($a_x$=$a_y$ in this case) of the orography are assumed to be 1.5 km and 250 km, respectively. The basic wind, which is assumed to be $U(z)$=(-15+0.004$z$) ms$^{-1}$ and $V(z)$=0 ms$^{-1}$, blows from east at the surface and reverses its direction at $z$=3.75 km. The Coriolis parameter is assumed to be $10^{-4}$ s$^{-1}$. This case is identical to that of Chen and Smith (1987) except that the basic wind is incident from the east-west direction instead of the north-south direction. Figure 21 shows the perturbation pressure, perturbation potential temperature, geostrophic vorticity, geostrophic vector wind fields at the surface and cross sections of the perturbation pressure and perturbation potential temperature along $y$=0 after 24 h. The basic features of the semigeostrophic model results are similar to the theoretical results of Smith (1984, 1986) and Chen and Smith (1987) and the nonlinear primitive equation model results of Lin and Perkey (1989). In the vicinity of the mountain top, an anticyclonic flow (Fig. 21d) develops, which is associated with the mountain-induced high pressure (Fig. 21a). The maximum perfurbation pressure is 2.2 mb. The mountain high is formed by the subgeostrophic flow of fluid particles approaching the mountain. Fluid particles are deflected slightly to the left upstream of the mountain if one faces downstream. This anticyclonic circulation is also shown in the geostrophic perturbation vorticity field (Fig. 21c). A pool of relatively cold air is associated with this mountain high (Fig. 21b). The perturbation temperature has a minimum of -4.0 K. The low, which has been advected by the mountain high, is formed in the northwest corner to the lee of the mountain (Fig. 21a). The minimum value of the perturbation pressure is -3.6 K. A similar pattern of positive perturbation temperature (warming) (Fig. 21b) is associated with the low. The perturbation temperature reaches a maximum value of 3.5 K. Notice that this pool of warm air is a combined effect of warm advection and downslope adiabatic warming. The cross sections of perturbation pressure and potential temperature (Figs. 21e and f) indicate that the forced baroclinic wave is shallow. Unlike the case of Lin and Perkey (1989), the blocking

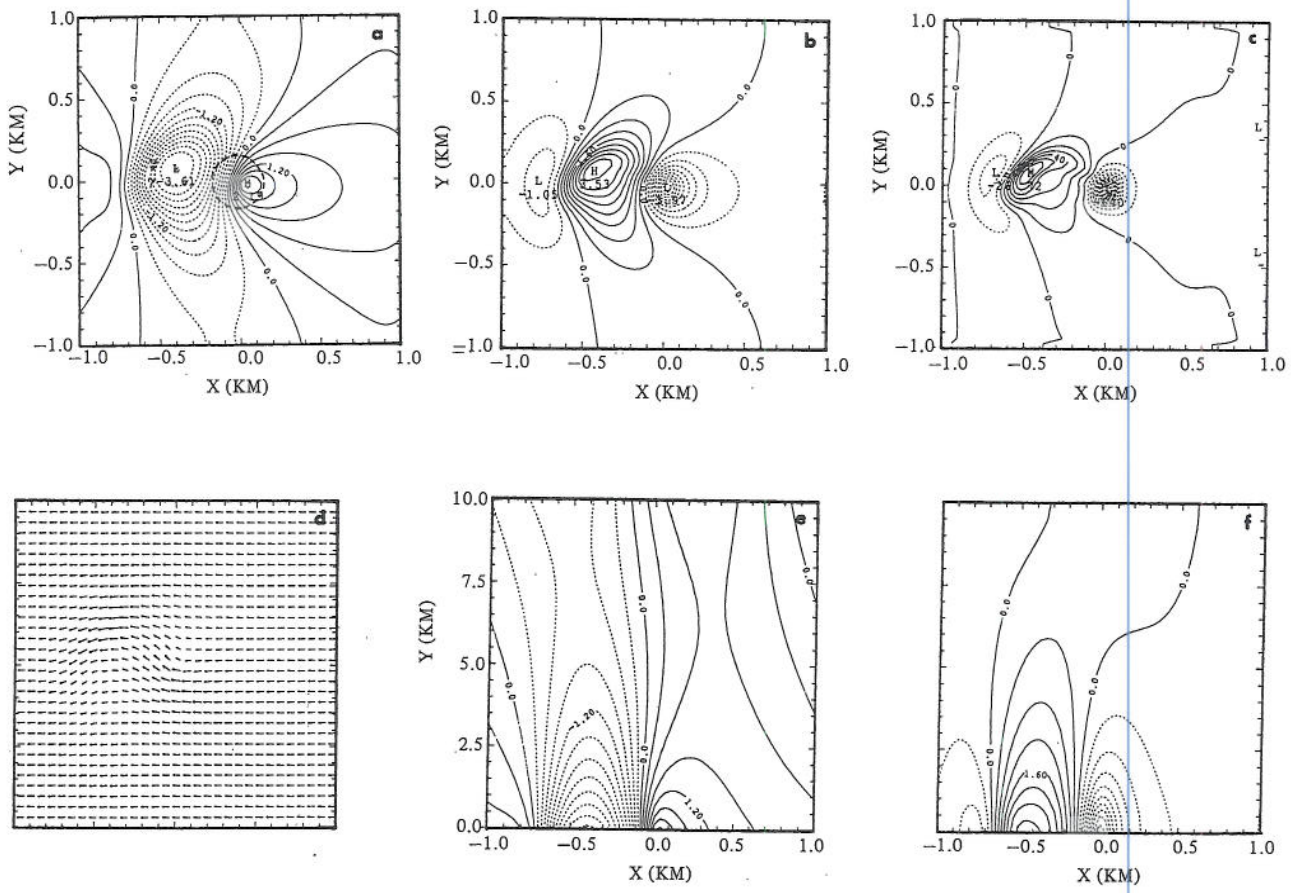


**Fig. 21.** Inviscid semigeostrophic continuously stratified baroclinic flow over a bell-shaped mountain with $h_o$=1.5 km and $a_x$=$a_y$=250 km. The basic wind is $U(z)$=(-15+0.004$z$) ms$^{-1}$ and $V(z)$=0 ms$^{-1}$, and blows from the east at the surface and reverses its direction at $z$=3.75 km. Other parameters are: $f$=$10^{-4}$ s$^{-1}$, $N$=0.01 s$^{-1}$, $T_o$=260 K, and $\rho_o$=1 kg m$^{-3}$. The dashed curve in (a) denotes the terrain contour of 360 m. Four horizontal fields at the surface after 24 h are shown: (a) perturbation pressure, (b) perturbation potential temperature, (c) geostrophic relative vorticity, and (d) vector wind. Vertical cross sections of perturbation pressure and potential temperature along $y$=0 are shown in (e) and (f), respectively.

effect is not pronounced in this case. This is due to the combined effect of the smaller mountain used and the neglect of the nonlinear ageostrophic advection of the ageostrophic wind.

Figure 22 shows the perturbation pressure, perturbation potential temperature, geostrophic vorticity, and geostrophic vector wind fields at the surface and cross sections of the perturbation pressure and perturbation potential temperature along $y$=0 after 24 h of a continuously stratified baroclinic flow over a bell-shaped heat source with circular contours. The diabatic heating function is prescribed by

$$q'(x,y)=\frac{Q_o}{[x^2/b_x^2+y^2/b_y^2+1]^{3/2}}, \qquad (95)$$

where $b_x$ and $b_y$ are the horizontal scales of the heat source in the $x$ and $y$ directions, respectively. The maximum heating rate ($Q_o$) and the horizontal scale ( $b_x$=$b_y$ in this case) of the heat source are assumed to be 0.24 J/kg-s and 150 km, respectively. The heating decreases with height exponentially with an e-folding value of 1.5 km. The basic wind, which is assumed to be $U(z)$=(-10+0.005$z$) ms$^{-1}$ and $V(z)$=0 ms$^{-1}$, blows from the east at the surface and reverses its direction at $z$=2 km. The Rossby number associated with this flow is about 0.33, which is estimated by $U_o/2fb_x$ with $U_o$=10 ms$^{-1}$, $f$=10$^{-4}$ s$^{-1}$, and $b_x$=$b_y$=150 km. Notice that we have used the whole width ($2b_x$) for the horizontal scale of the bell-shaped heat source, instead of the halfwidth. Hoskins (1975) places a loose upper limit on the Rossby number at $R_o$=0.5 for use in semigeostrophic theory. Therefore, the geostrophic momentum approximation may still be adquate for describing the flow in the present case. In response to this isolated diabatic heating, a region of low pressure with a minimum of about -3.19 mb forms in the vicinity of the heating region after 24 hr (Fig. 22a). There exists a much smaller region of relatively weak high pressure downstream of the concentrated heating region. Associated with the perturbation low and high pressures are more compact regions of warm and cold air, respectively (Fig. 22b). This is required by the hydrostatic equation. The low-high couplet associated with the forced baroclinic wave is lcated in the vicinity of the forcing region. The disturbance remains locally in the vicinity of the thermal forcing because the thermally forced baroclinic wave has a zero phase speed (Smith, 1984). At the

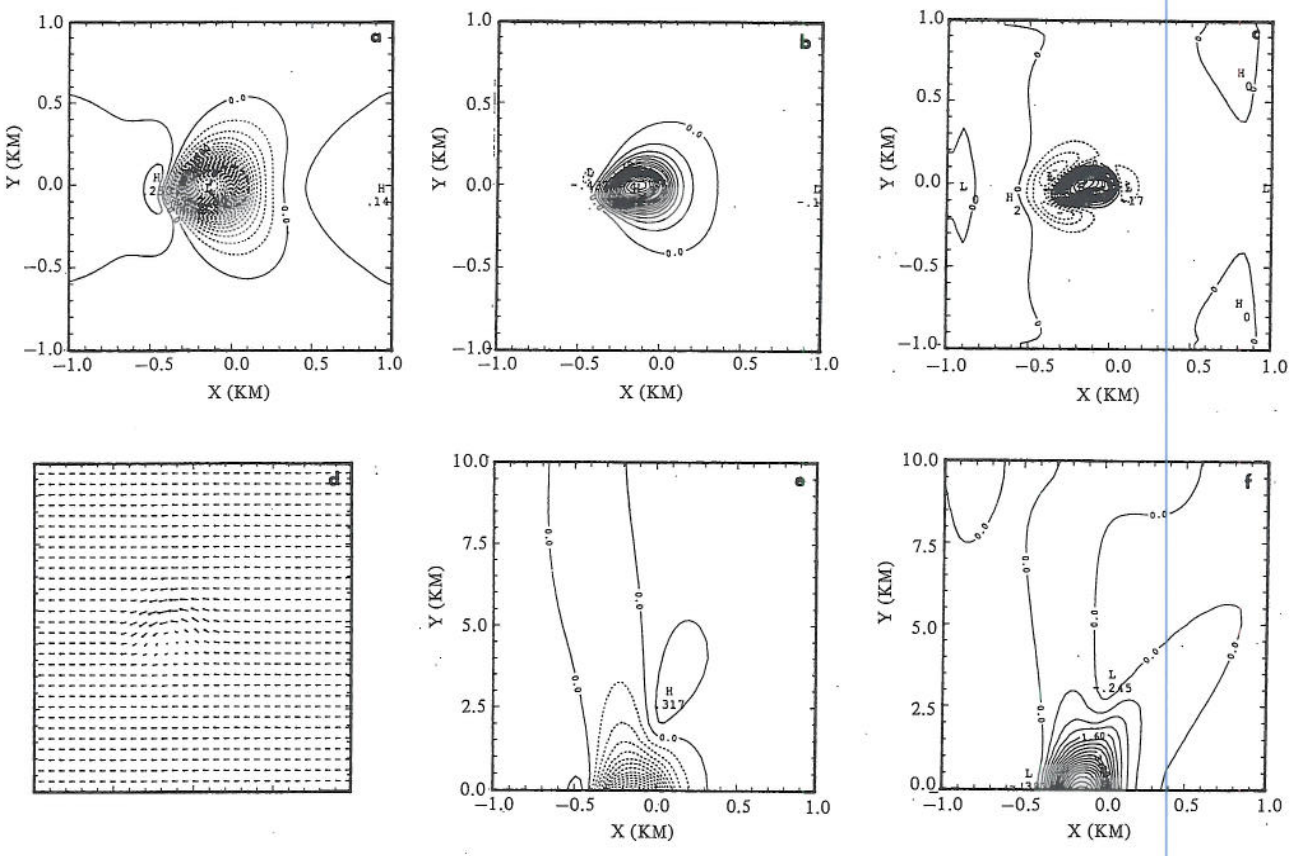


**Fig. 22.** Same as Fig. 21 except for flow over a bell-shaped heating region with $Q_o$=0.24 J (kg−s)$^{-1}$ and $b_x$=$b_y$=150 km. The heating rate of 0.04 J (kg−s)$^{-1}$ is denoted by the dashed curve in (a). The basic wind is $U(z)$=(-10+0.005$z$) ms$^{-1}$ and $V(z)$=0 ms$^{-1}$, and blows from the east at the surface and reverses its direction at $z$=2 km. The Rossby number associated with this flow is about 0.33.

surface, the fluid parcel experiences a cyclonic circulation near the center of the low pressure region, where there exists a cell of positive relative vorticity (Fig. 22c). A region of very weak negative vorticity is generated upstream of the heating, while a wider region of stronger negative vorticity is generated downstream of the heating. An inverted trough forms near the heating center (Fig. 22d), as is often observed to form along the Carolina coast in many cyclogenesis events. Both vertical cross sections of pressure and temperature fields (Figs. 22e and f) indicate that the disturbance is confined in a shallow layer. The present results are consistent with those with the assumption of shallow heating (Lin, 1989b, 1990a) except that the magnitude of the disturbance is weaker.

## IV. Concluding Remarks

In part II of this series of papers, we have reviewed the responses of a stably stratified shear flow to a mesoscale thermal forcing. Observations indicate that this type of shear flow is closely related to a number of mesoscale circulations. The mathematical method for solving a two-dimensional shear flow with a critical level to a prescribed thermal forcing was described. The mathematical problem was then extended to a three-dimensional flow and applied to the dynamics of mesoscale circulation associated with a mesoscale convective system. Generation and propagation of internal gravity waves by the heating were discussed. The mathematical problem was then extended to solve a stably stratified flow over a meso-$\alpha/\beta$ scale heat source. The vertical flux of horizontal momentum and wave energy associated with the thermally forced inertia-gravity waves have been described. Both quasi-geostrophic and semigeostrophic approaches to the problem were also reviewed. The solution was then applied to help understand the dynamics of coastal cyclogenesis.

In order to wholly understand the critical level effects in a nonrotating shear flow, the nonlinear effects should be included in the system. However, the present theory still provides significant physical insight into the problem. A more realistic treatment of the boundary layer processes should be used when one applies the present theories to predict the flow circulation associated with coastal cyclogenesis. In addition, the upper-level forcing, such as the jet streak, and the latent heating should also be considered.

### Acknowledgments

The author wishes to express his sincere appreciation to R. B. Smith of Yale University for introducing him to mesoscale dynamics, which helped to stimulate the series of work presented in this review. Discussions with R. F. Adler, A. Barcilon, C. Bretherton, C.-S. Chen, W.-D. Chen, D. R. Durran, K. Emanuel, G. M. Heymsfield, R. Hughes, G. S. Janowitz, D. Keyser, D. J. Raymond, R. Rotunno, and W.-Y. Sun among others were very helpful. The author is grateful to R. P. Weglarz and T.-A. Wang for reading the manuscript.

### References

Adler, R. F. and R. A. Mack (1986) Thunderstorm cloud top dynamics inferred from satellite observations and a cloud top parcel model. *J. Atmos. Sci.*, **43**, 1945-1960.

Adler, R. F., D. D. Fenn, and D. A. Moore (1981) Spiral feature observed at top of a rotating thunderstorm. *Mon. Wea. Rev.*, **109**, 194-199.

Anderson, C. E. (1982) Dramatic development of thunderstorm circulation associated with the Wichita Falls tornado as revealed by satellite imagery. Twelveth Conf. on Severe Local Storms, San Antonio, Amer. Meteor. Soc., 493-498.

Anthes, R. A., Y.-H. Kuo, and J. R. Gyakum (1983) Numerical simulations of a case of explosive marine cyclogenesis. *Mon. Wea. Rev.*, **111**, 1174-1188.

Bannon, P. R. (1986) Linear development of quasi-geostrophic baroclinic disturbances with condensational heating. *J. Atmos. Sci.*, **43**, 2261-2274.

Bannon, P. (1990) Comments on "A theory of cyclogenesis forced by diabatic heating. Part I: A quasi-geostrophic approach". *J. Atmos. Sci.*, **47**, 2241-2242.

Bjerknes, J. (1951) *Compendium of Meteorology*, T. F. Malone, Ed., pp. 577-598. Amer. Meteor. Soc., U.S.A.

Bluestein, H. B. and M. H. Jain (1985) Formation of mesoscale lines of precipitations: Severe squall lines in Oklahoma during spring. *J. Atmos. Sci.*, **42**, 1711-1732.

Booker, J. R. and F. P. Bretherton (1967) The critical layer for internal gravity waves in a shear flow. *J. Fluid Mech.*, **27**, 513-539.

Bosart, L. F. (1981) The presidents' Day snowstorm of 18-19 February 1979: A subsynoptic scale event. *Mon. Wea. Rev.*, **109**, 1542-1566.

Bosart, L. F. (1988) Coastal frontogenesis and cyclogenesis during GALE IOP#2. GALE/CASP Workshop Reports, 75-93.

Bretherton, F. P. (1966) The propagation of groups of internal gravity waves in a shear flow. *Quart. J. Roy. Meteor. Soc.*, **92**, 466-480.

Buzzi, A. and S. Tibaldi (1977) Inertial and frictional effects on rotating and stratified flow over topography. *Quart. J. Roy. Meteor. Soc.*, **103**, 135-150.

Charney, J. G. and A. Eliassen (1949) A numerical method for predicting the perturbations of the middle-latitude westerlies. *Tellus*, **1**, 38-54.

Chen, W.-D. and R. B. Smith (1987) Nonlinear semigeostrophic lee cyclogenesis. Sixth Extratropical Cyclone Workshop, Monterey, CA.

Chun, H.-Y. (1991) Role of a critical level in a shear flow with diabatic heating. Ph.D. Dissertation, North Carolina State University, U.S.A.

Crook, N. A. and M. W. Moncrieff (1988) The effect of large-scale convergence on the generation and maintenance of deep moist convection. *J. Atmos. Sci.*, **45**, 3606-3624.

Eady, E.T. (1949) Long waves and cyclone waves. *Tellus*, **3**, 36-52.

Eliassen, A. (1962) On the vertical circulation in frontal zones. *Geofys. Publ.*, **24**, 147-160.

Eliassen, A. and E. Palm (1960) On the transfer of energy in stationary mountain waves. *Geofys. Publ.*, **22**, 1-23.

Estoque, M. A. (1962) The sea breeze as a function of the prevailing synoptic situation. *J. Atmos. Sci.*, **19**, 244-250.

GALE (1986) Genesis of Atlantic Low Experiment field project summary. T. J. Mercer and C. W. Kreitzberg, Eds., GALE Data Center, Drexel University, Philadelphia, U.S.A.

Gill, A. E. (1982) *Atmosphere-Ocean Dynamics*. 622 pp. Int. Geophys. Ser., Vol. 30, Academic Press, U.S.A.

Gossard, E. E. and W. H. Hooke (1975) *Waves in the Atmosphere*. 456 pp, Elsevier Scientific, U.S.A.

Heymsfield, G. M. and R. H. Blackmer, Jr. (1988) Satellite-observed

characteristics of Midwest severe thunderstorm anvils. *Mon. Wea. Rev.*, **116**, 2200-2224.

Heymsfield, G. M., R. H. Blackmer, Jr., and S. Schotz (1983a) Upper level structure of Oklahoma tornadic storms on May 2, 1979: Part I. *J. Atmos. Sci.*, **40**, 1740-1755.

Heymsfield, G. M., G. Szejwach, S. Schotz, and R. H. Blackmer, Jr. (1983b) Upper level structure of Oklahoma tornadic storms on May 2, 1979: Part II. *J. Atmos. Sci.*, **40**, 1756-1767.

Heymsfield, G. M., R. Fulton, and J. D. Spinhirne (1991) Aircraft overflight measurements of midwest severe storms: Implications on geosynchronous satellite interpretations. *J. Atmos. Sci.*, **119**, 436-456.

Hoskins, B. J. (1975) The geostrophic momentum approximation and the semi-geostrophic equations. *J. Atmos. Sci.*, **32**, 233-242.

Hsu, H.-M. (1987a) Study of linear steady atmospheric flow above a finite surface heating. *J. Atmos. Sci.*, **44**, 186-199.

Hsu, H.-M. (1987b) Mesoscale lake-effect snowstorms in the vicinity of Lake Michigan: Linear theory and numerical simulations. *J. Atmos. Sci.*, **44**, 1019-1040.

Jones, W. L. (1967) Propagation of internal gravity waves in fluids with shear flow and rotation. *J. Fluid Mech.*, **30**, 439-448.

Klemp, J. B. and D. K. Lilly (1978) Numerical simulation of hydrostatic mountain waves. *J. Atmos. Sci.*, **35**, 78-107.

Klemp, J. B. and R. B. Wilhelmson (1978) The simulation of three-dimensional convective storm dynamics. *J. Atmos. Sci.*, **35**, 1070-1096.

Koch, S. E. and P. B. Dorian (1988) A mesoscale gravity wave event observed during CCOPE. Part III: Wave environment and probable source mechanisms. *Mon. Wea. Rev.*, **116**, 2570-2592.

LeBlond, P. H. and L. A. Mysak (1978) *Waves in the Ocean*. 602 pp., Elsevier Scientific, U.S.A.

Lighthill, M. J. (1970) *Introduction to Fourier Analysis and General Functions*. 79 pp., Cambridge University Press, U.S.A.

Lin, Y.-L. (1986a) Calculation of airflow over an isolated heat source with application to the dynamics of V-shaped clouds. *J. Atmos. Sci.*, **43**, 2736-2751.

Lin, Y.-L. (1986b) A study of the transient dynamics of orographic rain. *Pap. Meteor. Res.*, **9**, 19-45.

Lin, Y.-L. (1987) Two-dimensional response of a stably stratified flow to diabatic heating. *J. Atmos. Sci.*, **44**, 1375-1393.

Lin, Y.-L. (1989a) Inertial and frictional effects on stratified hydrostatic airflow past an isolated heat source. *J. Atmos. Sci.*, **46**, 921-936.

Lin, Y.-L. (1989b) A theory of cyclogenesis forced by diabatic heating. Part I: A quasi-geostrophic approach. *J. Atmos. Sci.*, **46**, 3015-3036.

Lin, Y.-L. (1990a) A theory of cyclogenesis forced by diabatic heating. ı art II: A semi-geostrophic approach. *J. Atmos. Sci.*, **47**, 1755-1777.

Lin, Y.-L. (1990b) Reply to Bannon's comments on "A theory of cyclogenesis forced by diabatic heating. Part I: A quasi-geostrophic approach". *J. Atmos. Sci.*, **47**, 2243-2244.

Lin, Y.-L. (1994) Airflow over mesoscale heat sources. Part I: Responses in a uniform flow. *Proc. Natl. Sci. Counc. ROC(A)*, **18**(1), 1-32.

Lin, Y.-L. and H.-Y. Chun (1991) Effects of diabatic cooling in a shear flow with a critical level. *J. Atmos. Sci.*, **48**, 2476-2491.

Lin, Y.-L. and D. J. Perkey (1989) Numerical modeling studies of a process of lee cyclogenesis. *J. Atmos. Sci.*, **46**, 3685-3697.

Lin, Y.-L. and S. Li (1988) Three-dimensional response of a shear flow to elevated heating. *J. Atmos. Sci.*, **45**, 2987-3002.

Lin, Y.-L. and R. B. Smith (1986) Transient dynamics of airflow near a local heat source. *J. Atmos. Sci.*, **43**, 40-49.

Lin, Y.-L., R. D. Farley, and H. D. Orville (1983) Bulk parameterization of the snow field in a cloud model. *J. Climate Appl. Meteor.*, **22**, 1065-1092.

Lin, Y.-L., N.-H. Lin, and R. P. Weglarz (1992) Numerical modeling studies of lee mesolows, mesovortices and mesocyclones with application to the formation of Taiwan mesolows. *Meteor. Atmos. Phys.*, **49**, 43-67.

Lindzen, R. S. (1974) Wave-CISK in the tropics. *J. Atmos. Sci.*, **31**, 156-179.

Lindzen, R. S. and K.-K. Tung (1976) Banded convective activity and ducted gravity waves. *Mon. Wea. Rev.*, **104**, 1602-1617.

Luthi, D., C. Schar, and H. C. Davies (1989) On the atmospheric response to steady mesoscale low-level diabatic heating. *Contri. Atmos. Phys.*, **62**, 126-150.

Malkus, J. S. and M. E. Stern (1953) The flow of a stable atmosphere over a heat island. Part. I. *J. Meteor.*, **10**, 30-41.

Marwitz, J. D. (1972) The structure and motion of severe hailstorms. Part I: Supercell storms. *J. Appl. Meteor.*, **11**, 166-179.

Maslowe, S. A. (1986) Critical layers in shear flows. *Ann. Rev. Fluid Mech.*, **18**, 405-432.

Negri, A. J. (1982) Cloud-top structure of tornadic storms on 10 April, 1979 from rapid scan and stereo satellite observations. *Bull. Amer. Meteor. Soc.*, **63**, 1151-1159.

Newton, C. W. (1966) Circulations in large sheared cumulonimbus. *Tellus*, **18**, 699-712.

Nicholls, M. E., R. A. Pielke, and W. R. Cotton (1991) Thermally forced gravity waves in an atmosphere at rest. *J. Atmos. Sci.*, **48**, 1869-1884.

Ogura, Y. and Y.-L. Chen (1977) A life history of an intense mesoscale convective storm in Oklahoma. *J. Atmos. Sci.*, **34**, 1458-1476.

Ogura, Y. and M.-T. Liou (1980) The structure of a midlatitude squall line: A case study. *J. Atmos. Sci.*, **37**, 553-567.

Orlanski, I. and J. J. Katzfey (1987) Sensitivity of model simulations for a coastal cyclone. *Mon. Wea. Rev.*, **115**, 2792-2821.

Pedlosky, J. (1982) *Geophysical Fluid Dynamics*. 2nd ed., 624 pp., Springer-Verlag, U.S.A.

Pierrehumbert, R. T. and B. Wyman (1985) Upstream effects of mesoscale mountains. *J. Atmos. Sci.*, **42**, 977-1003.

Queney, P. (1947) Theory of perturbations in stratified currents with applications to air flow over mountain barriers. Dept. Meteor., Univ. of Chicago, Misc. Report No. 23, 81 pp.

Ramage, C. S. (1971) *Monsoon Meteorology*. 296 pp., Academic Press, NY, U.S.A.

Raymond, D. J. (1984) A wave-CISK in mass flux form. *J. Atmos. Sci.*, **41**, 1946-1958.

Raymond, D. J. (1986) Prescribed heating of a stratified atmosphere as a model for moist convection. *J. Atmos. Sci.*, **43**, 1011-1111.

Raymond, D. J. and R. Rotunno (1989) Response of a stably stratified flow to cooling. *J. Atmos. Sci.*, **46**, 2830-2837.

Rhea, J. O. (1966) A study of thunderstorm formation along dry lines. *J. Appl. Meteor.*, **5**, 58-63.

Rotunno, R. (1983) On the linear theory of the land- and sea-breeze. *J. Atmos. Sci.*, **40**, 1999-2005.

Rotunno, R., J. B. Klemp, and M. L. Weisman (1988) A theory for strong, long-lived squall lines. *J. Atmos. Sci.*, **45**, 463-485.

Schlesinger, R. E. (1980) A three-dimensional numerical model of an isolated thunderstorm. Part II. *J. Atmos. Sci.*, **37**, 395-420.

Schlesinger, R. E. (1984) Mature thunderstorm cloud-top structure and dynamics: A three-dimensional numerical simulation study. *J. Atmos. Sci.*, **41**, 1551-1570.

Schlesinger, R. E. (1988) Effects of stratospheric lapse rate on thunderstorm cloud top structure in a three-dimensional numerical simulation. Part I. *J. Atmos. Sci.*, **45**, 1555-1570.

Seitter, K. L. and H.-L. Kuo (1983) The dynamical structure of a squall-line type thunderstorm. *J. Atmos. Sci.*, **40**, 2831-2854.

Smagorinsky, J. (1953) The dynamical influence of large-scale heat sources and sinks on the quasi-stationary mean motions of the atmosphere. *Quart. J. Roy. Meteor. Soc.*, **79**, 342-366.

Smith, R. B. (1979) The influence of mountains on the atmosphere. *Adv. in Geophys.*, **21**, Ed. B. Saltzman, Academic Press, NY, 87-230.

Smith, R. B. (1980) Linear theory of stratified hydrostatic flow past an isolated mountain. *Tellus*, **32**, 348-364.

isolated mountain. *Tellus*, **32**, 348-364.
Smith, R. B. (1984) A theory of lee cyclogenesis. *J. Atmos. Sci.*, **41**, 1159-1168.
Smith, R. B. (1986) Further development of a theory of lee cyclogenesis. *J. Atmos. Sci.*, **43**, 1582-1602.
Smith, R. B. (1989) Comment on "Low Froude number flow past three-dimensional obstacles. Part I". *J. Atmos. Sci.*, **46**, 3611-3613.
Smith, R. B. and Y.-L. Lin (1982) The addition of heat to a stratified airstream with application to the dynamics of orographic rain. *Quart. J. Roy. Meteor. Soc.*, **108**, 353-378.
Smith, R. B. and Y.-L. Lin (1983) Orographic rain on the Western Ghats. *Mountain Meteorology*, Eds. E. R. Reiter *et al.*, pp. 71-94. Sci. Press and Amer. Meteor. Soc., U.S.A.
Smolarkiewicz, P. K. and R. Rotunno (1989) Low Froude number flow past three-dimensional obstacles. Part I. *J. Atmos. Sci.*, **46**, 1154-1164.
Sun, W.-Y. and Y. Ogura (1979) Boundary layer forcing as a possible trigger to a squall-line formation. *J. Atmos. Sci.*, **36**, 235-254.
Thorpe, A. J., M. J. Miller, and M. W. Moncrieff (1980) Dynamical models of two-dimensional downdraughts. *Quart. J. Roy. Meteor. Soc.*, **106**, 463-484.
Thorpe, A. J., M. J. Miller, and M. W. Moncrieff (1982) Two-dimensional convection in a nonconstant shear: A model of mid-latitude squall lines. *Quart. J. Roy. Meteor. Soc.*, **108**, 739-762.
Uccellini, L. W. and P. J. Kocin (1987) The interaction of jet streak circulations during heavy snow events along the East Coast of the United States. *Wea. Forecasting*, **1**, 289-308.
Uccellini, L. W., P. J. Kocin, R. A. Peterson, C. H. Wash, and K. F. Brill (1984) The Presidents' Day cyclone of 18-19 February 1979: Synoptic overview and analysis of the subtropical jet streak influencing the precyclogenetic period. *Mon. Wea. Rev.*, **112**, 31-55.
Wyss, J. and K. A. Emanuel (1988) The pre-storm environment of midlatitude prefrontal squall lines. *Mon. Wea. Rev.*, **116**, 790-794.

# 由熱力作用下所引發的中尺度環流的動力現象 第二部份：在有風切氣流場的反應

林玉郎

海洋、地球與大氣科學系
美國北卡羅來納州立大學

## 摘　要

在本文第二部份裡，我們將綜覽穩定成層風切氣流對熱源的反應。有些觀測顯示出這類風切氣流和一些中尺度環流有相當密切之關係。在文內，我們將詳述二維含臨界層之風切氣流對固定熱源的數學解，此類數學解將被延伸到三維氣流上，並應用到中尺度對流系統的環流動力上。同時，我們也將討論內重力波之產生及傳播。穩定成層氣流通過對大的或中的中尺度熱源的反應也可應用類似的數學解法。在敍述此類解法時和慣性重力波有關的水平動量之垂直傳播及波動能量也將被詳述，並應用至沿岸旋生的動力問題上。